Paused Pol II Coordinates Tissue Morphogenesis in the Drosophila Embryo

Mounia Lagha, Jacques P Bothma, Emilia Esposito, Samuel Ng, Laura Stefanik, Chiahao Tsui, Jeffrey Johnston, Kai Chen, David S Gilmour, Julia Zeitlinger, et al.

Cell

Paused Pol II Coordinates Tissue Morphogenesis in the *Drosophila* Embryo

Mounia Lagha,[1,5] Jacques P. Bothma,[2,5] Emilia Esposito,[1] Samuel Ng,[1] Laura Stefanik,[3] Chiahao Tsui,[1] Jeffrey Johnston,[4] Kai Chen,[4] David S. Gilmour,[3] Julia Zeitlinger,[4] and Michael S. Levine[1,*]

[1]Department of Molecular and Cell Biology
[2]Biophysics Graduate Group
University of California, Berkeley, Berkeley, CA 94720, USA
[3]Center for Gene Regulation, Department of Biochemistry and Molecular Biology, The Pennsylvania State University, University Park, PA 16802, USA
[4]Stowers Institute for Medical Research, Kansas City, MO 64110, USA
[5]These authors contributed equally to this work
*Correspondence: mlevine@berkeley.edu
http://dx.doi.org/10.1016/j.cell.2013.04.045

SUMMARY

Paused RNA polymerase (Pol II) is a pervasive feature of *Drosophila* embryos and mammalian stem cells, but its role in development is uncertain. Here, we demonstrate that a spectrum of paused Pol II determines the "time to synchrony"—the time required to achieve coordinated gene expression across the cells of a tissue. To determine whether synchronous patterns of gene activation are significant in development, we manipulated the timing of *snail* expression, which controls the coordinated invagination of ~1,000 mesoderm cells during gastrulation. Replacement of the strongly paused *snail* promoter with moderately paused or non-paused promoters causes stochastic activation of *snail* expression and increased variability of mesoderm invagination. Computational modeling of the dorsal-ventral patterning network recapitulates these variable and bistable gastrulation profiles and emphasizes the importance of timing of gene activation in development. We conclude that paused Pol II and transcriptional synchrony are essential for coordinating cell behavior during morphogenesis.

INTRODUCTION

The early *Drosophila* embryo is the premier system for visualizing gene activity in animal development. In a period of just 1 hr, broadly distributed maternal determinants generate localized patterns of gene activity, including segmentation stripes of gene expression (Chen et al., 2012). A variety of studies suggest that enhancers, typically 300–500 bp in length, are responsible for determining where and when developmental control genes are switched on and off (Ong and Corces, 2011). With few exceptions, localized patterns of expression can be attributed to discrete enhancers located upstream, downstream, or within the gene of interest.

The enhancer is therefore seen as the key agent of differential gene activity in animal development (Ong and Corces, 2011). Considerably less is known about the role of the promoter in the regulation of the spatial or temporal limits of gene expression, although they are known to control the rates of RNA synthesis (Juven-Gershon and Kadonaga, 2010). In the simplest view, enhancers determine the limits of gene expression (where and when genes are active), whereas the promoter controls the levels of expression (e.g., how many transcripts are produced in a given unit of time).

The purpose of this study is to determine whether the promoter regions of developmental control genes can influence the timing or spatial limits of gene expression in the early *Drosophila* embryo. We were motivated by the recent finding that many developmental control genes contain paused RNA polymerase (Pol II) prior to their activation during embryogenesis (Adelman and Lis, 2012; Levine, 2011). The function of paused Pol II is uncertain, despite its apparent prevalence (~30% of all protein coding and noncoding genes) in both *Drosophila* embryos and mammalian stem cells (Guenther and Young, 2012).

The prototypic example of paused Pol II, *Drosophila* heat shock genes, underlies rapid induction of gene expression in response to stress (Boehm et al., 2003). There is also evidence that paused Pol II serves to keep promoters "open" by excluding or diminishing the occurrence of positioned nucleosomes that occlude the transcription start site in cultured cells (Gilchrist et al., 2010). Recent quantitative imaging methods suggest that paused Poll II influences synchronous induction of gene expression across the different cells of presumptive tissues in the early *Drosophila* embryo (Boettiger and Levine, 2009).

In the latter study, quantitative in situ hybridization assays were used to detect the first nascent transcripts encoded by different developmental control genes, within the first 10–20 min after the onset of expression in precellular embryos,

~2 hr after fertilization. Genes were classified as synchronous if nascent transcripts were detected in over 50% of the nuclei that will eventually express a given gene or stochastic if expressed in fewer than 50%. Most paused genes exhibited synchronous patterns of activation, whereas most nonpaused genes displayed stochastic expression. The evidence linking paused polymerase and synchrony was strictly correlative, and there is no evidence that these modes of activation are significant in development.

Here, we employ quantitative imaging (Bothma et al., 2011; Perry et al., 2010), whole-genome Pol II-binding assays (Zeitlinger et al., 2007), and BAC transgenesis (Venken et al., 2006) to examine the function of paused Pol II in the early *Drosophila* embryo. Evidence is presented that minimal promoter sequences, ~100–200 bp centered around the +1 transcription start site, are sufficient for establishing paused Pol II and mediating rapid, synchronous activation of gene expression in transgenic embryos. Those genes containing high levels of paused Pol II achieve coordinate expression more rapidly than those containing low levels.

To determine whether the "time to synchrony" is important in development, we manipulated the coordinate expression of *snail* (*sna*) (*Slug*/*Sna2* in vertebrates), a major determinant of epithelial-mesenchyme transitions (EMTs) in animal development. In *Drosophila*, *sna* is expressed in ~1,000 cells comprising the presumptive mesoderm (Kosman et al., 1991; Leptin and Grunewald, 1990). These cells undergo coordinated invagination during gastrulation, within 90 min of the onset of *sna* expression (Leptin, 2005; Sweeton et al., 1991). To determine whether synchronous activation of *sna* expression is essential for coordinated invagination of the mesoderm, we replaced the native *sna* promoter with those from moderately paused (*short gastrulation*; *Chordin*) or nonpaused (*thisbe*; *Fgf8*) genes. These heterologous promoters result in less synchronous patterns of *sna* activation and a progressive reduction in mesoderm invagination during gastrulation. We therefore conclude that paused Pol II and transcriptional synchrony are essential for coordinating cell behavior during morphogenesis.

RESULTS

Previous studies suggested a correlation between paused Pol II and synchronous patterns of gene activation in the *Drosophila* embryo. Moreover, computational analyses identified sequence elements that are associated with promoters containing paused Pol II, including GAGA and pause button (PB) motifs (e.g., Gilchrist et al., 2010; Hendrix et al., 2008; Lee et al., 2008; Shopland et al., 1995). These observations raise the possibility that the core promoter might be sufficient to determine whether a gene is paused or not paused and activated in a synchronous or stochastic fashion.

As a first step toward testing this possibility, we examined the regulation of two Dpp (BMP) target genes, *pannier* (*pnr*; *GATA4*) and *tailup* (*tup*; *Islet-1*), transcription factors essential for the specification of a variety of dorsal tissues, including the heart (Vincent and Buckingham, 2010). These genes are coactivated in the dorsal ectoderm of 2 hr embryos (e.g., Ashe et al., 2000) but, nonetheless, display opposite Pol II-binding profiles. *tup* is strongly paused, whereas *pnr* lacks Pol II (Zeitlinger et al., 2007). The use of quantitative imaging methods revealed differences in their activation profiles that were missed in previous studies, as discussed below (Figure 1).

Temporal Coordination of Dpp Target Genes

tup is activated by high levels of the Dpp gradient, whereas *pnr* is triggered by low levels (Figures 1A–1H) (Ashe et al., 2000). These distinctive spatial expression patterns depend on previously identified *tup* and *pnr* enhancers. Quantitative imaging methods reveal that they also exhibit dissimilar temporal profiles (Figures 1E–1I).

It was previously shown that *tup* contains paused Pol II and is activated in a synchronous fashion, whereas *pnr* lacks Pol II and exhibits stochastic expression (Boettiger and Levine, 2009). We developed high-resolution confocal visualization and image segmentation methods to measure the time to synchrony, i.e., the degree of temporal coordination in gene activation during nuclear cleavage cycle (cc) 14, the 1 hr interval preceding gastrulation (Figures 1A–1H). The ~6,000 cells comprising the pregastrula embryo are synchronized within the cell cycle, thereby permitting direct comparisons of transcriptional coordination. Quantitative FISH assays permit detection of nascent transcripts shortly after the onset of gene expression (e.g., Bothma et al., 2011). In this assay, activation is defined as the time it takes for 50% of the nuclei to express nascent transcripts (t50). Using a cumulative gamma distribution, we fit a curve to each experimental data set (see Figure S1 available online; Supplemental Information). t50 values are calculated by measuring the fraction of nuclei that express a given gene for each fitted activation profile. Pregastrula cc14 embryos are selected based on nuclear density and embryo morphology and then ordered relative to one another based on the fraction of the expression pattern containing nascent transcripts. The collections are designed to ensure that embryos are distributed in an unbiased way across the entirety of cc14. This approach allows us to measure the t50 values with an accuracy of ±5 min (see Table 1; Figure S1; Table S1; Supplemental Information).

The endogenous *tup* and *pnr* genes exhibit distinct t50 activation profiles: *tup* achieves t50 expression ~26 min after the onset of cc14, whereas *pnr* does not exhibit comparable expression for another 15 min (Table 1). This represents a significant delay because the entire cc14 interphase extends for just 55 min (see below). To determine whether these divergent temporal expression profiles are due to enhancer or promoter sequences, we created a BAC transgene encompassing the entire *tup* transcription unit and flanking regulatory DNAs that recapitulates the rapid and synchronous activation profile of the endogenous *tup* locus (Figures 1J and S2). In these experiments, the *tup* transcription unit was replaced with the *yellow* reporter gene to facilitate detection of nascent transcripts (Perry et al., 2010). There is a slight delay in the t50 value of the BAC transgene (~32 min) as compared with the endogenous *tup* locus (~26 min) (Table 1), which is likely due to the heterologous site of transgene insertion, a slower rate of *yellow* transcription, or the use of heterozygous embryos to measure expression of BAC transgenes (see Figures 1I and 1J).

We next examined the activation profile obtained upon replacement of the paused *tup* promoter (*tupPr*) with the

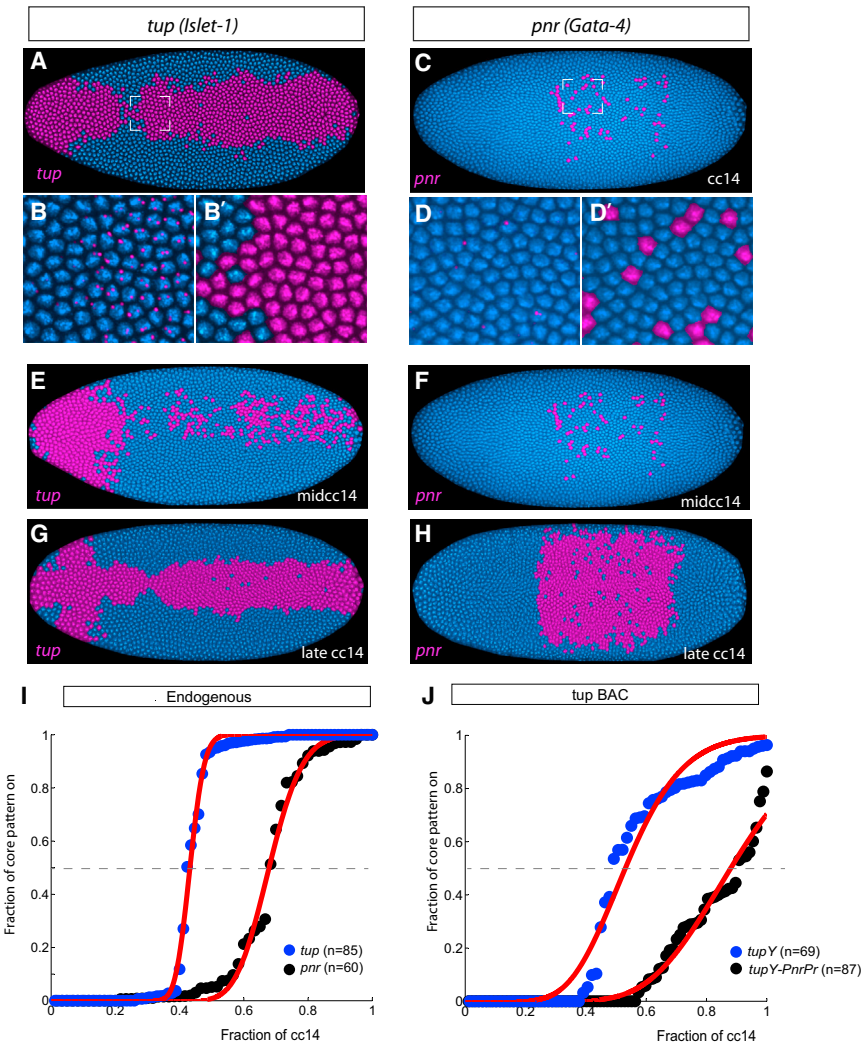

Figure 1. BMP/Dpp Target Genes Exhibit Distinct Coordination Profiles

(A–H) cc14 embryos hybridized with *tup* and *pnr* fluorescent (magenta) intronic probes for detecting nascent transcripts (nuclei stained with DAPI [blue]). Raw images for *tup* and *pnr* transcripts are shown in (B) and (D), and the corresponding processed images are shown in (B′) and (D′). Images shown in (B) and (D) are magnifications of bracketed regions in (A) and (C). (E–H) *tup* (E and G) and *pnr* (F and H) expression during mid (E and F) and late (G and H) cc14.

(I and J) Dynamics of gene expression during cc14 based on the fraction of nuclei containing nascent transcripts. (I) Endogenous *tup* expression (blue) reaches 50% of the complete pattern (t50, 26) 15 min earlier than does *pnr* (black) (t50, 41). (J) There is a delay in *tup* dynamics when the minimal promoter of a *tup* BAC transgene (*tupY*) is replaced by that of *pnr* (*tupY-PnrPr*) (see also Figure S2). The red curves represent the fitted curves (using a cumulative gamma distribution) to the data depicted in (I) and (J) (see Supplemental Information; Figure S1; Table S1). t50 values are determined from these fitted curves.

Minimal Promoter Sequences Are Sufficient to Establish Paused Pol II

The preceding results suggest that minimal promoter sequences might be sufficient to determine whether a gene is activated in a synchronous or stochastic fashion. To establish whether they are also sufficient for determining the presence or absence of paused Pol II, we analyzed minigenes containing the *pnr* intronic enhancer (*pnrE*), *tupPr*, and *yellow* reporter gene (*pnrE* > *tupPr*/*yellow*). This minigene exhibits synchronous expression in the dorsal ectoderm of wild-type embryos (see below) but is inactive in *Toll*^{10b} mutants due to the absence of Dpp signaling (Schneider et al., 1991). Both the endogenous *tup* locus and the minigene nonetheless contain paused Pol II in these "silent" *Toll*^{10b} embryos (Figures 2A and 2B); as expected, the endogenous *pnr* locus lacks paused Pol II (Zeitlinger et al., 2007) (Table S2). Permanganate footprint assays identified hypersensitive thymidine residues at positions +48 and +51 nucleotides downstream of the *tup* transcription start site in transgenic embryos (Figure 2C), strengthening the evidence that the stalled Pol II identified at the *tupPr* represents promoter-proximal paused Pol II.

Thus, the 200 bp *tupPr* region is sufficient for the establishment of paused Pol II (and synchronous expression, as shown below). It contains key signatures of paused promoters (Gilchrist et al., 2010; Hendrix et al., 2008; Lee et al., 2008; Shopland et al., 1995), including 5′ GAGA elements located ~100 bp upstream of the transcription start site, and PB motifs positioned +54 to +64 bp downstream of the start site, in the vicinity of the hypersensitive thymidine residues identified by permanganate

nonpaused *pnr* promoter (Figures 1J and S2). The modified BAC transgene is identical to the control, except for the substitution of just 200 bp centered around the +1 transcription start site of the *pnr* promoter (Figure S3). The modified transgene was inserted into the same chromosomal location as the control transgene, thereby permitting direct quantitative comparisons of their activation dynamics. Surprisingly, this 200 bp substitution within the large 60 kb BAC transgene is sufficient to convert the rapid and synchronous *tup-yellow* expression pattern into a slow and stochastic mode of activation (Figure 1J).

The modified transgene exhibits a t50 value of 53 min, which is considerably slower than the t50 values seen for the endogenous *tup* locus (26 min) or unmodified *tup* BAC transgene (32 min). It is somewhat slower than the t50 value seen for the endogenous *pnr* locus (41 min), although the differential timing of the *tup* versus *pnr* promoters (Δt50) is similar for the endogenous loci and BAC transgenes, at 15 and 21 min, respectively (Table 1). These findings suggest that the *pnr* promoter, not enhancers, is the prime determinant of its slow and stochastic activation profile during development.

Table 1. Summary of the t50 Values for All of the Constructs Used in This Study

Promoter	t50 Time (min)	Uncertainty from Simulations (min)
PnrPr Endo	41	3
TupPr Endo	26	3
Tup-Y BAC	32	3
Tup-Y-PnrPr BAC	53	2
PnrE-TupPr NelfE/Spt5	39	4
PnrE-TupPrShort	31	3
PnrE-TupPr Trl	30	4
PnrE-TupPr	15	3
PnrE-SnaPr	24	3
PnrE-Hsp70Pr	28	4
PnrE-SogPr	38	4
PnrE-ThsPr	55	2
PnrE-PnrPr	74	4
SnaE-SnaPr	3	2
SnaE-SogPr	22	4
SnaE-ThsPr	40	3
SnaE-PnrPr	42	3
SogE-TupPr	1	0.6
SogE-SnaPr	1	0.6
SogE-PnrPr	35	7

t50 corresponds to the time it takes for an embryo to show nascent transcription in 50% of the pattern. t50 is an estimated time based on the measured activated kinetics of many embryos (see also Figure S1 and Table S1).

protection assays (Figures 2C and S3). We therefore conclude that minimal promoter sequences are sufficient to establish paused Pol II in vivo, in the *Drosophila* embryo. In principle, any gene can be artificially "paused" or "depaused" by exchanging minimal promoter sequences. Such an approach may be relevant to the stem cell field because some of the key determinants of pluripotency (e.g., Nanog) exhibit stochastic expression among the different ICM cells of mouse embryos (Kalmar et al., 2009; Nichols and Smith, 2011).

Promoter-Associated Elements Influence Transcriptional Synchrony

To establish a sharper connection between "pausing elements" in the *tupPr* and transcriptional synchrony, we expressed the *pnrE* > *tupPr/yellow* transgene in embryos containing diminished levels of the GAGA-binding protein, GAF (or Trl). Previous studies implicated GAGA and Trl in the stable association of paused Pol II within the proximal promoter of *Hsp70* (Fay et al., 2011; Lee et al., 1992; Shopland et al., 1995). The *tupPr* region contains GAGA elements located ~100 bp upstream of the transcription start site (Figure S3), and whole-genome assays confirm GAF/Trl binding to this region in the *Drosophila* embryo (Schuettengruber et al., 2009). Reduced levels of Trl caused an ~20 min delay in the activation of the *pnrE* > *tupPr/yellow* transgene, as compared with wild-type embryos (Figure 2D; Table1), similar to the activation profile mediated by the nonpaused *thisbe* promoter (see below). An equivalent delay is observed with a truncated *tupPr* lacking upstream GAGA elements but retaining all core elements such as the INR (Figure 2D; Table1). These studies suggest a close correlation between Trl/GAGA and the temporal coordination of gene activation.

The stability of paused Pol II also depends on negative elongation factors, such as NELF and Spt5, which bind nascent transcripts shortly after the onset of transcription (Gilchrist et al., 2010; Li and Gilmour, 2011). There is an ~30 min delay in the activation profile of the *pnrE* > *tupPr/yellow* transgene in embryos containing reduced levels of NelfE and Spt5 (Figure 2D; Table1). Thus, the preceding findings suggest a close correlation among minimal promoter sequences, paused Pol II, and the time to synchrony in the *Drosophila* embryo.

A Spectrum of Synchrony

Whole-genome Pol II chromatin immunoprecipitation sequencing (ChIP-seq) assays suggest that genes might not be simply paused or nonpaused, and activated in a strictly synchronous or stochastic fashion. Instead, there are different levels of Pol II in the promoter regions of genes previously identified as stalled or not stalled (Figure 3F; see Zeitlinger et al., 2007). Normalized levels of paused Pol II were measured in vivo in dorsal-ventral patterning mutants containing a single embryonic tissue, in which the gene in question is silent (Figure 3F). For example, *tup* is not expressed in $Toll^{10b}$ mutant embryos because they contain only mesoderm due to the transformation of ectoderm into mesoderm. Conversely, *sna* is not expressed in gd^{7} mutant embryos, which display the reciprocal transformation of mesoderm into ectoderm. The *tup* and *sna* promoters contain significantly more Pol II sequence reads than *sog* in silent mutant embryos, even though all three genes were classified as stalled or paused in previous studies (Zeitlinger et al., 2007). Similarly, *thisbe* contains more Pol II than *pnr*, even though both genes were classified as nonstalled. *tup* is consistently seen to contain the highest levels of promoter-proximal Pol II read counts in a variety of tissues (Gaertner et al., 2012).

To investigate the significance of these different levels of Pol II, we analyzed the expression of a series of minigenes containing the *pnr* enhancer (*pnrE*) and six different promoter sequences encompassing a spectrum of paused Pol II (Figure S3). Remarkably, the activation profiles of these minigenes mirror the levels of Pol II binding (Figure 3E; Table 1). The *tupPr* contains the highest levels of Pol II and exhibits a t50 value of just ~15 min. This is followed by progressively slower profiles for *sna* (t50, 24 min), *hsp70* (28 min), and *sog* (38 min), which contain successively lower levels of Pol II.

Finally, the promoter regions of the nonpaused genes *ths* and *pnr* exhibit the slowest activation dynamics, although *ths* is somewhat faster (t50, 55 min) than *pnr* (t50, 74 min). A similar correlation between the levels of paused Pol II and the time to synchrony was seen for minigenes containing the *sog* intronic enhancer, which mediates activation in the neurogenic ectoderm (Figures S4A–S4D; Table1), and for the distal *sna* enhancer (*snaE*) in the mesoderm (see below).

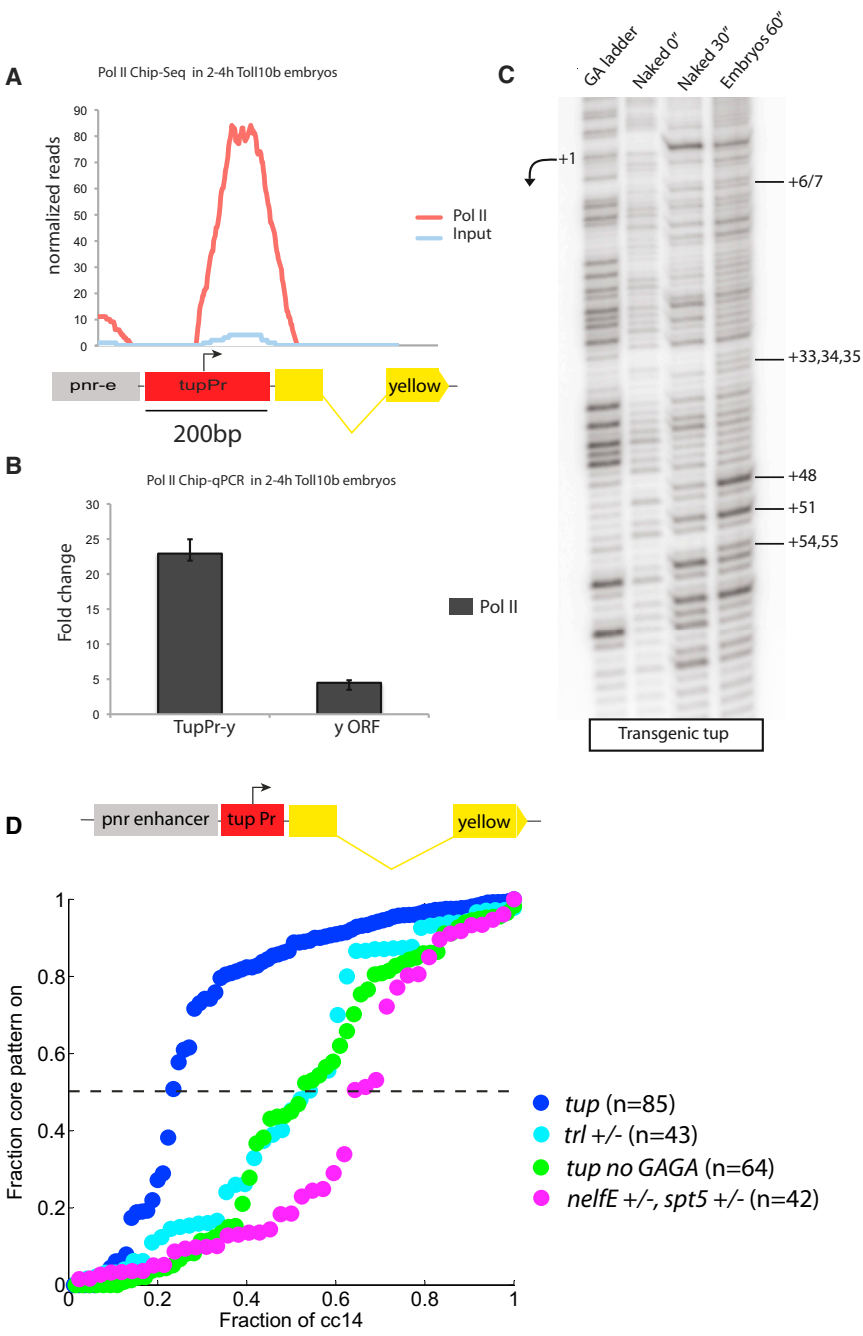

Figure 2. The Minimal Promoter Mediates Paused Pol II

(A) Pol II Chip-seq reads of the *pnr/tup* transgene in a tissue where it is silent.

(B) Pol II ChIP followed by qPCR showing enrichment at the *tupPr/yellow* junction. y ORF, yellow open reading frame. Error bars represent SD.

(C) Permanganate footprinting reveals a promoter-proximal "transcription bubble" in mutant embryos where the *tupPr/yellow* transgene is silent.

(D) Reduced levels of maternal *Trl* (turquoise) or *NelfE/Spt5* (pink) cause a delay in the expression profile of the *pnr*E > *tupPr* transgene. A similar effect is observed with a truncated version of the *tupPr* lacking the upstream GAGA sites.

See also Figure S3 for relevant promoter sequences.

Transcriptional Synchrony and Rates of RNA Synthesis

The preceding findings demonstrate that the same enhancer can produce a spectrum of activation profiles in the ectoderm of early embryos. To determine the feasibility of manipulating the timing of gene expression in the presumptive mesoderm, we placed the distal (shadow) *snaE* (Dunipace et al., 2011; Perry et al., 2010) upstream of the *sna*, *sog*, *ths*, and *pnr* promoters and *yellow* reporter gene (Figures 4A–4C). We observed similar relative t50 values as those obtained with the *pnrE* (Figure 3; Table 1). The *sna* promoter mediates a t50 value of 3 min, whereas the more weakly paused *sog* promoter exhibits a 19 min delay in the t50 profile (Figure 4D; Table 1). As expected, the nonpaused *ths* and *pnr* promoters mediate even slower activation profiles (t50, 40 and 42 min, respectively). The *snaE* mediates more rapid onset of expression in cc14 than the *pnrE*, probably due to the earlier availability of activators (e.g., Dorsal and Twist) in the mesoderm as compared with the dorsal ectoderm (e.g., pSmad). Nonetheless, after upstream activators initiate expression, the detailed temporal dynamics (t50 activation) are determined by the different promoter sequences.

The *sna*, *sog*, and *ths* promoters provide a nice spectrum of activation during cc14 (t50 values of 3, 22, and 40 min, respectively) and seem ideally suited for manipulating the synchrony of *sna* expression in the presumptive mesoderm. Our choice of *sna* stems from the short lag time, less than 90 min, between the onset of transcription and morphogenesis—the coordinate invagination of the ventral mesoderm during gastrulation (see below). However, the accurate interpretation of any changes in gastrulation arising from the use of heterologous promoters requires an understanding of the relationship between t50 activation profiles and the levels of gene expression.

We expected promoters mediating slow synchrony profiles (e.g., *ths*) to produce weaker expression than those mediating rapid synchrony (e.g., *sna* promoter). Single-molecule in situ hybridization (smFISH) assays (Boettiger and Levine, 2013) were employed to measure the number of *yellow* mRNAs produced by different yellow minigenes: *snaE* > *pnrPr/yellow*, *snaE* > *thsPr/yellow*, and *snaE* > *snaPr/yellow* (Figure 4E). As expected, the "slow" minigenes produce lower levels of *yellow* mRNAs

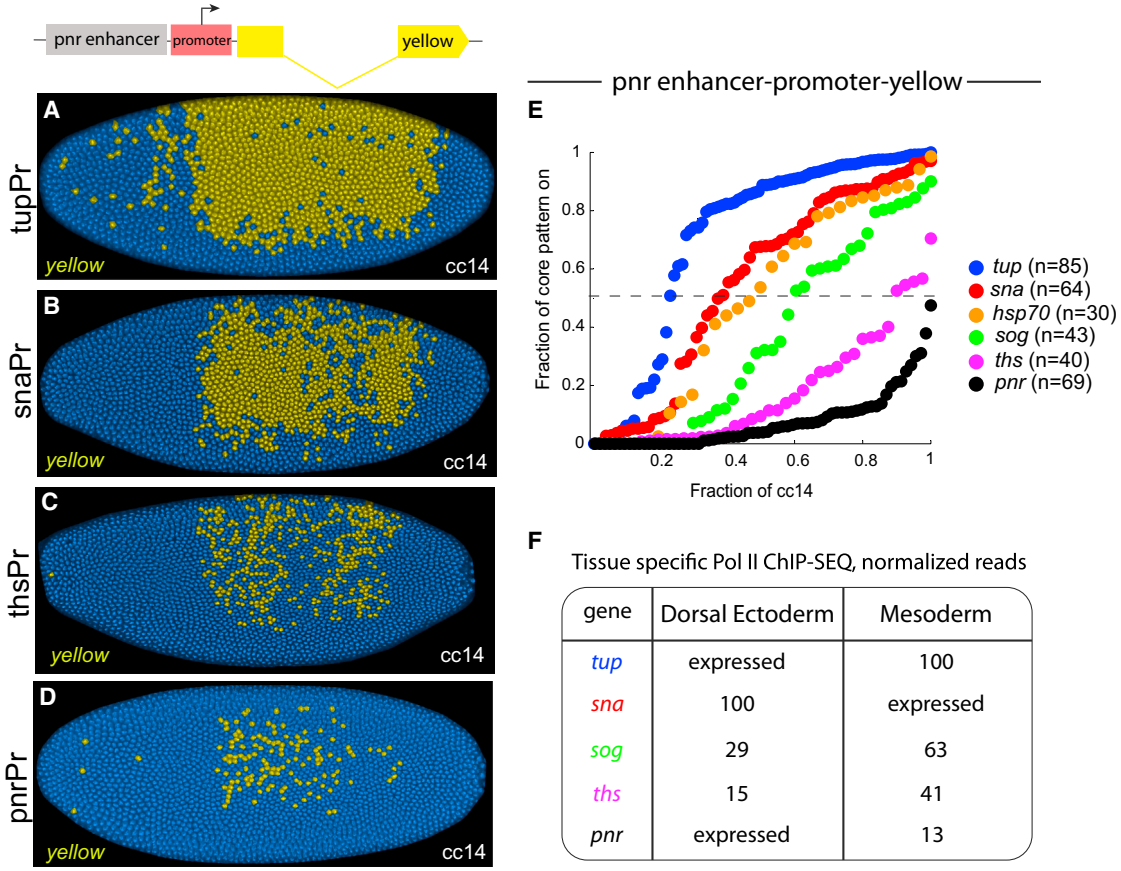

gene	Dorsal Ectoderm	Mesoderm
tup	expressed	100
sna	100	expressed
sog	29	63
ths	15	41
pnr	expressed	13

Figure 3. A Spectrum of Synchrony

The *pnrE* was placed upstream of the *tup*, *sna*, *Hsp70*, *sog*, *ths*, and *pnr* promoters (Pr) (see diagram in upper left).

(A–D) Examples of transgenic embryos stained with a *yellow* intronic probe at the midpoint of cc14. The *tupPr* mediates synchronous expression in the dorsal ectoderm (A), whereas the *pnrPr* mediates stochastic expression (D).

(E) Temporal coordination profiles during cc14. The *tupPr* provides the rapid coordination profile, whereas the *pnr* promoter exhibits the slowest coordination. *Sog* and *ths* give intermediate.

(F) Relative amounts of Pol II at the promoter regions of inactive genes. For actively expressed genes, we denote them as "expressed"; the normalized Pol II reads are provided in Table S2.

than the "fast" genes. The *pnr*, *ths*, and *sna* promoters produce 30 ± 10, 60 ± 20, and 100 ± 30 mRNAs per cell, respectively, in the mesoderm prior to invagination.

Modeling methods were used to estimate promoter strength based on activation kinetics (see Supplemental Information; Figures S4E–S4I). The different levels of *yellow* mRNAs produced by the *ths* and *sna* promoters can be attributed to their respective t50 activation profiles. The *snaE > thsPr/yellow* minigene is expressed at lower levels than *snaE > snaPr/yellow* due to its slower synchrony profile. However, once activated in a given cell, the *ths* promoter appears to mediate a similar rate of RNA synthesis as the *sna* promoter (see Supplemental Information; Figures S4E–S4I). Similarly, quantitative measurements suggest that the *sog* promoter mediates a similar rate of expression as the *sna* and *ths* promoters once activated (see below). In contrast, the low levels of *yellow* mRNAs produced by the *pnr* promoter probably result from the combination of a slow synchrony profile and a lower rate of RNA synthesis. Thus, we focused on the use of the *ths* and *sog* promoters to examine the consequences of "desynchronizing" the onset of *sna* expression.

Transcriptional Synchrony Is Essential for Coordinate Invagination

A 25 kb *sna* BAC transgene encompassing the *sna* transcription unit, proximal enhancer, and neighboring *Tim17B2* locus (which harbors the distal *sna* shadow enhancer) was shown to be sufficient to rescue the gastrulation defects of sna^{-}/sna^{-} mutant embryos (Dunipace et al., 2011; Perry et al., 2010). However, there is evidence that the proximal enhancer might attenuate *sna* expression by impeding access of the distal enhancer to the *sna* promoter (Dunipace et al., 2011) (data not shown). Consequently, we removed this enhancer in order to obtain a more direct assessment of the contributions of the different promoters in coordinating mesoderm invagination. It is important to note that the distal enhancer is sufficient for complete rescue of the gastrulation defects of sna^{-}/sna^{-} mutant embryos and the development of fully viable adult flies (Dunipace et al., 2011).

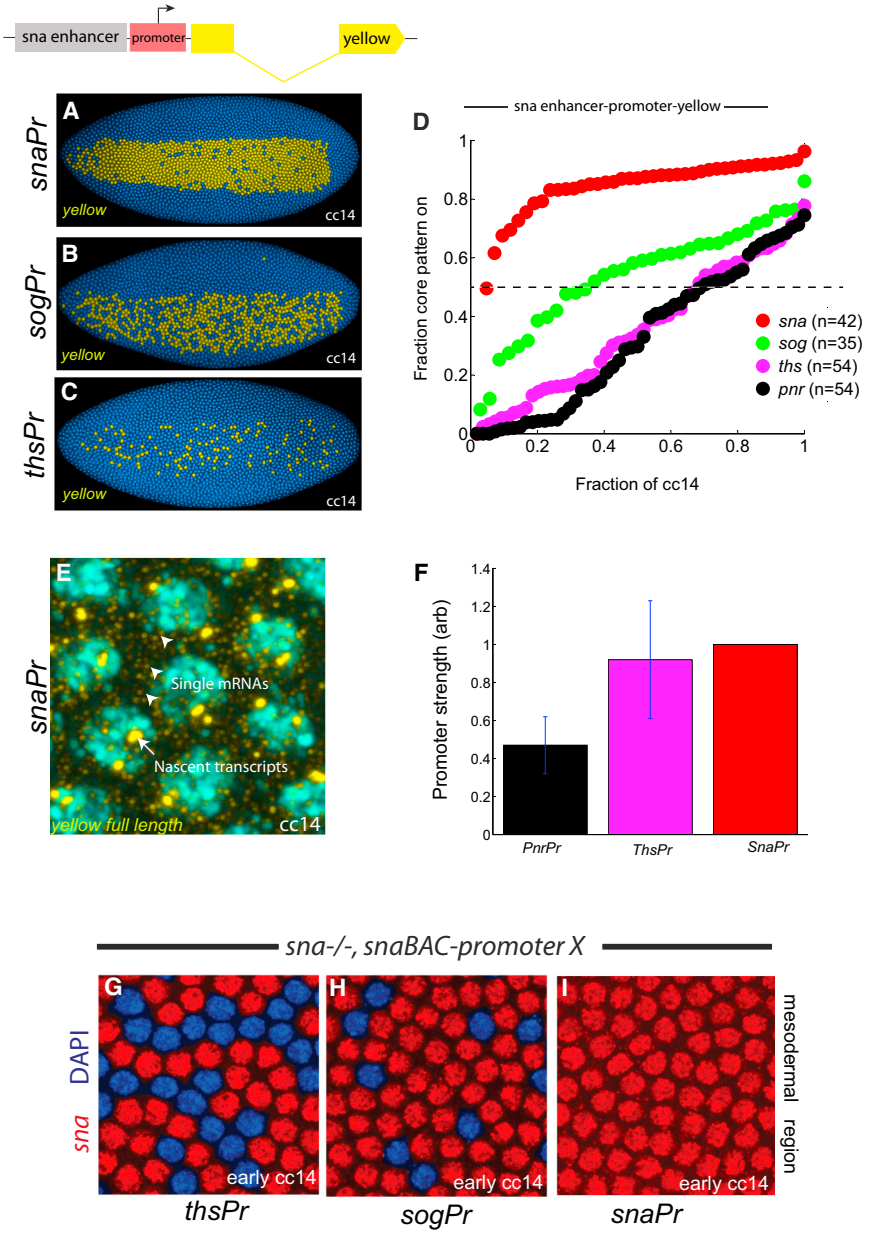

Figure 4. Minimal Promoters Are Sufficient to Perturb *sna* Temporal Coordination

The distal *snaE* was placed upstream of the *snaPr* (A), *sogPr* (B), and *thsPr* (C) promoters attached to the *yellow* reporter gene (see diagram in upper left).

(A–C) Processed images after FISH using a *yellow* intronic probe.

(D) Temporal coordination profiles during cc14.

(E) High-resolution confocal image of *yellow* mRNAs encoded by the *snaE* > *snaPr/yellow* minigene. Arrowheads point to individual cytoplasmic mRNAs; arrow indicates nascent transcripts.

(F) Bar graph showing the estimated promoter strength from the *pnr*, *ths*, and *sna* promoters just prior to gastrulation (see Experimental Procedures and Figure S4). Error bars represent SD. a.u., arbitrary units.

(G–I) False-colored nuclei showing the presence of nascent transcripts for *sna* in the rescue BAC constructs containing the *ths* (G), *sog* (H), and *sna* (I) promoter.

(Figures 5A–5D). In contrast, the transgene containing the moderately paused *sog* promoter produces truncated furrows (Figures 5E, 5F, and 5H) (18 out of 22) but occasionally induces nearly complete furrows approaching those seen in wild-type embryos (Figures 5G and 5G′) (4 out of 22). Finally, the nonpaused *ths* promoter produces highly variable phenotypes, ranging from the complete absence of invagination (11 out of 16), to erratic pockets of ingressing cells (3 out of 16) (Figures 5I and 5J), and rarely, extended grooves of invaginating cells (2 out of 16) (Figures 5K and 5K′). Snail mRNAs and protein are detected only in the invaginating cells of partially rescued embryos exhibiting truncated furrows or isolated pockets of ingression (Figures 5D, 5H, 5L, and S5A–S5F). These studies suggest that the time to synchrony is a critical determinant of coordinate cell behavior in development (see below).

We employed recombineering methods to create a series of *sna* BAC transgenes that contain either *sog* or *ths* promoter sequences in place of the native *sna* promoter (replacement of ~100–110 bp; see Figure S3). The three BAC transgenes (native *sna* promoter, *sog* promoter, or *ths* promoter) exhibit distinctive patterns of activation during the onset of cc14 (Figures 4G–4I), concomitant with the levels of paused Pol II and the t50 synchrony values seen for the *sna* minigenes (Figures 4A–4D).

There is a tight correlation between these activation profiles and the extent to which mesoderm invagination is rescued in sna^{-}/sna^{-} embryos (Figure 5). Thus, the "native" transgene containing the strongly paused *sna* promoter mediates a coordinated ventral furrow and robust invagination of the mesoderm

Computational Models of Gastrulation Variability

We constructed a mathematical model (Figures 6A–6C) to explain the highly variable gastrulation phenotypes seen for the *sna* BAC transgenes containing the *sog* and *ths* promoters. Bistability of *sna* expression is often observed in the anterior third of the embryo encompassing ~300 of the ~1,000 cells comprising the ventral furrow (e.g., Figures 5E′, 5F′, and 5K′). This model makes use of the wealth of knowledge about the transcription networks governing the dorsal-ventral patterning of the *Drosophila* embryo (reviewed by Rushlow and Shvartsman, 2012). It also draws on recent dynamic imaging of the Dorsal

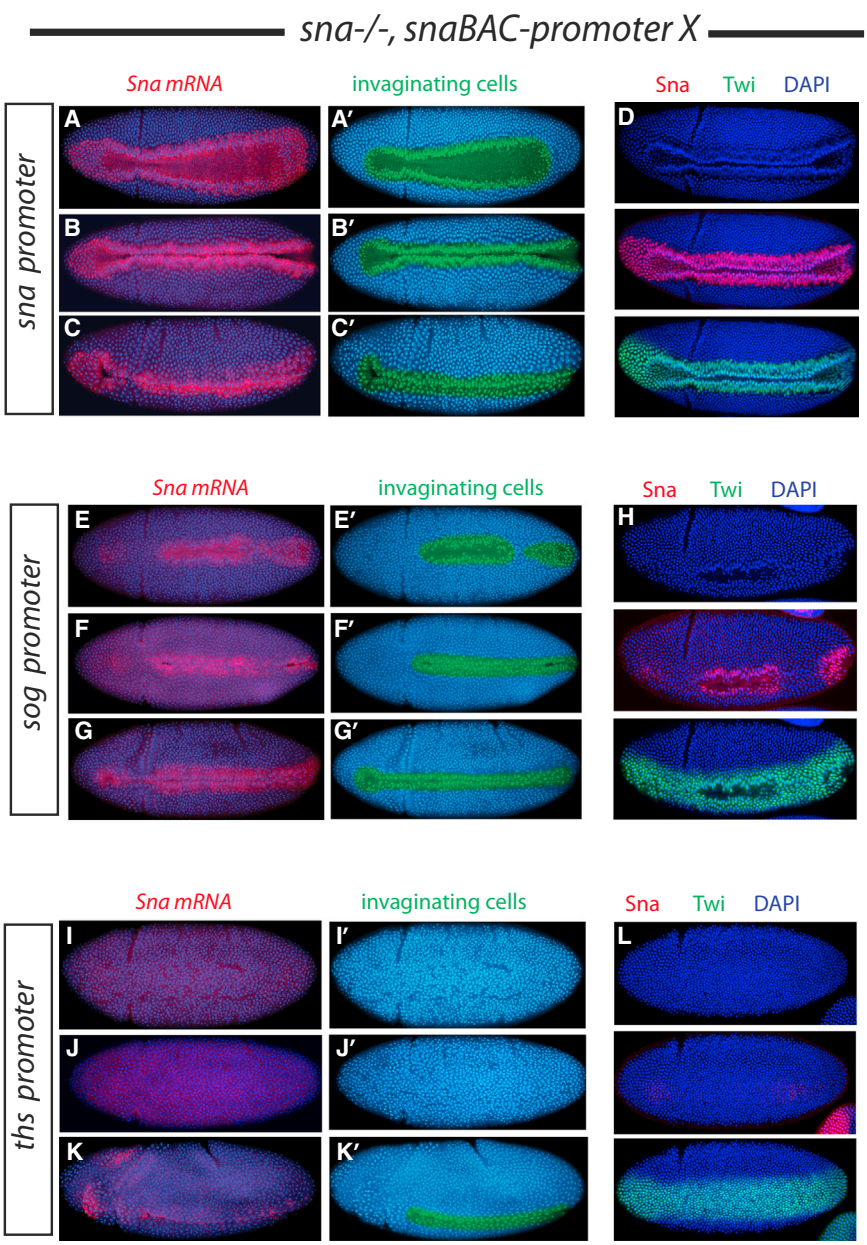

Figure 5. Stochastic Expression of *sna* Results in Gastrulation Defects

(A–L) Transgenic rescue embryos stained with a *sna* probe (in red) at gastrulation stages (A–C, E–G, and I–K) and correspondent invaginating cells false colored in green (A′–C′, E′–G′, and I′–K′).

(A–C) When *sna* expression is driven by a snaBAC-sna promoter lacking the primary enhancer, all embryos gastrulate normally.

(E–G) Variable gastrulation defects are obtained when the *sna* promoter is replaced by the moderately paused *sog* promoter. Most embryos show pockets of ingressing cells (E and E′), and "half furrow" (F and F′) and occasional embryos show a normal furrow (G and G′).

(I–K) When *sna* is artificially depaused by replacing its promoter by the *ths* promoter sequence, most embryos fail to gastrulate (I–J′), but rare embryos exhibit an extended groove of invaginating cells (K and K′).

(D, H, and L) Transgenic embryos stained with sna (red) and twist (Twi; green) antibodies at gastrulation when the ventral furrow is invaginating.

See also Figure S5.

nuclear gradient (Kanodia et al., 2009, 2011; Liberman et al., 2009; Reeves et al., 2012), which revealed a slight narrowing of the gradient in anterior regions. Our model also invokes sna autoregulation, which is suggested by the rapid loss of *sna* transcripts (Hemavathy et al., 1997) and *yellow* transcripts from a *sna* BAC transgene (Figures S5G–S5J) in sna^{-}/sna^{-} null embryos. We explored different mechanisms of autoregulation and obtained the most faithful results with an indirect model, whereby Snail represses a localized ectodermal repressor via a double-negative feedback loop (see Supplemental Information; Figure S6).

Computational simulations consistently produce uniform ventral furrows when the onset of *sna* expression is rapid and uniform (t50, 0–4 min after the onset of cc14) (Figures 6C and 6D), as seen for the native *sna* promoter (Figure 4I). However, slightly less coordinated patterns of activation (t50, 4–7 min), e.g., *sog* promoter (Figure 4H), produce highly variable ventral furrows (Figure 6E). As the coordination is further reduced (t50, 7–12 min) (Figure 6F), most simulations show a complete loss of the furrow, although a small fraction of simulations produce half furrows in the posterior half of the embryo, as seen for the *ths* promoter (Figures 4G and 5K).

The bistable, all or none invagination of the anterior mesoderm can be explained by the combination of reduced levels of the Dorsal gradient, variable activation of Snail expression, and delayed synthesis of critical threshold levels of the Snail repressor (Figures 6E and 6F). The key insight from these simulations is that short-range diffusion among neighboring nuclei can produce sufficient levels of Snail repressor to rescue small but not large patches of *sna*-expressing nuclei. The decision to maintain or repress *sna* expression occurs during a very tight time window, ~10–20 min after the onset of gastrulation. The key parameter underlying bistability is the time to synchrony because similar results are obtained when computer simulations are performed with a range of Hill coefficients for *sna* regulation and different diffusion rates for the Snail protein (see Figure S7).

DISCUSSION

Through a combination of BAC transgenesis, whole-genome ChIP assays, quantitative imaging, and computational modeling,

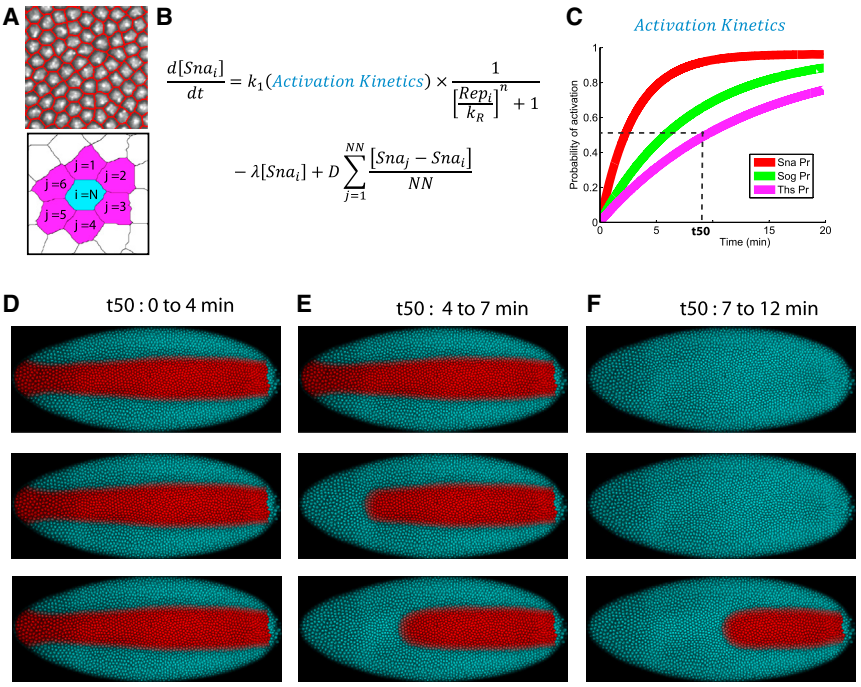

Figure 6. Modeling Gastrulation Variability: The Importance of Coordination

(A) Mesodermal region of a DAPI-stained embryo to show the segmentation process of the nuclei. The panel below is a schematic illustrating the neighbors (j) of a given mesodermal nucleus (i). We allow for nearest neighbor diffusion, where the "i" nucleus is diffusively coupled to its nearest neighbors that share a boundary (j, 1:6 in this case).

(B) Simplified mathematical model for Snail dynamic expression in a given nucleus (i). The key parameters are the timing of sna activation in the particular nuclei, the concentration of the neurogenic repressor (Rep), and the concentration of activators like Dorsal (k1), number of nearest neighbors (NN), and the strength of the diffusive coupling between nuclei (D).

(C) Activation curves computationally obtained for three different promoters: *sna*, *sog*, and *ths*.

(D–F) Results of computational simulations when *sna* temporal coordination is affected; t50 values are indicated.

See also Figures S5, S6, and S7.

we obtained evidence that the time to synchrony is a critical determinant of coordinate cell behavior in the *Drosophila* embryo. Genes containing high levels of paused Pol II are activated in a more rapid and coordinated fashion than those containing intermediate or low levels. It is conceivable that paused Pol II will prove to be an essential feature of other patterning processes requiring rapid coordination of gene expression and cell behavior. For example, pausing of Notch signaling components (e.g., *Hes*) might help coordinate expression of the "clock" genes underlying somitogenesis in vertebrate embryos (Saga, 2012), which occurs on a timescale similar to mesoderm specification and invagination in *Drosophila* (~90 min from the onset of sna transcription to the formation of the ventral furrow).

Model for the Developmental Timing of Gene Activation

Recent studies in S2 cells suggest that developmentally regulated genes tend to contain either paused Pol II or inhibitory nucleosomes (Gilchrist et al., 2010). RNAi-mediated depletion of NELF led to reduced levels of paused Pol II and a concomitant increase in promoter-positioned nucleosomes. These studies prompted the proposal that paused Pol II might render genes poised for activation by excluding the formation of inhibitory nucleosomes at the core promoter.

It is possible that nonpaused genes mediate slow activation dynamics due to cell-cell variation in the eviction of inhibitory nucleosomes at the core promoter. If occupied by an inhibitory nucleosome, a distal enhancer will not be able to stimulate transcription as it engages the promoter. Either the enhancer must await repositioning or dynamic turnover of inhibitory nucleosomes to allow recruitment of Pol II. Either way, this process might be inherently stochastic, resulting in cell-to-cell variations in the onset of transcription.

In principle, this model can account for the spectrum of activation profiles seen for genes containing different levels of paused Pol II. A gene containing high levels, such as *tup*, is more likely to contain Pol II than an inhibitory nucleosome in a given cell at a given time as compared with genes containing little or no paused Pol II (e.g., *ths* and *pnr*, respectively). Consequently, upon induction, strongly paused genes exhibit synchronous patterns of activation because most of the promoters in the different cells of a tissue contain Pol II. In contrast, genes containing little or no paused Pol II are more likely to contain an inhibitory nucleosome in a given cell at a given time, resulting in variable delays in the onset of gene expression. Thus, the ratio of poised and inhibited states might determine the time to synchrony.

The *sna* gene contains lower levels of Pol II than the *tupPr* (Gaertner et al., 2012). When attached to the *pnrE*, it mediates a t50 activation profile of 24 min (Table 1), which is similar to the prototypic paused *hsp70* promoter but significantly slower than the *tupPr* (15 min) (see Figure 3). Recent studies in cultured cells suggest that transcription initiation can be dissociated from subsequent rounds of Pol II recruitment for p53 target genes, resulting in rapid rates of activation but low steady-state levels of mRNAs (Morachis et al., 2010). It has been suggested that strongly paused genes are not necessarily expressed at high levels due to the dwelling of Pol II within the proximal promoter at every round of transcription following activation (Gilchrist et al., 2012; Lin et al., 2011). This could reduce the rate of RNA synthesis by lowering the frequency of elongating Pol II complexes. In contrast, promoters containing weaker pausing elements might achieve higher loading of Pol II complexes due to shorter dwell times.

We propose that there is a "trade-off" between timing and levels of gene expression at paused genes. Genes containing

moderate levels of paused Pol II, such as *hsp70* and *sna*, might achieve an optimal balance between excluding inhibitory nucleosomes for synchronous activation and efficient loading of Pol II complexes. Evidence for this model is seen for the *tupPr*. It mediates rapid and synchronous activation of a *sna* BAC transgene but significantly weaker expression than the *sna* promoter (see Figures S5K–S5M).

Dynamic Control of the Dorsal-Ventral Patterning Network

The gene regulatory network underlying the spatial control of dorsal-ventral patterning has been extensively studied (reviewed by Rushlow and Shvartsman, 2012). Considerably less is known about the temporal dynamics of this process. Indeed, developmental timing has only recently become a critical focus of study, even in well-defined systems such as the patterning of the vertebrate neural tube (Balaskas et al., 2012). Here, we have shown that perturbing coordinate activation of the *sna* expression pattern leads to various invagination defects during gastrulation. Computational modeling (Figure 6) highlights the importance of timing in producing these defects. Delayed and asynchronous patterns of activation uncouple Snail from the other components of the dorsal-ventral patterning network, resulting in variable gaps and bistability of the ventral furrow, particularly in the anterior mesoderm. Indeed, this uncoupling results in the expression of high levels of the Dorsal and Twist activators in regions that fail to invaginate due to the delay in Snail expression (e.g., Figures 5H and 5L). This uncoupling of *sna* expression from its activators provides a vivid illustration of the importance of temporal dynamics in the control of complex developmental processes. A static gene network based on a simple Dorsal gradient affinity model does not appear to be sufficient to capture the intricacies of mesoderm morphogenesis.

The dorsal-ventral patterning network amplifies small changes in the levels of the dynamic Dorsal gradient to produce all or none patterns of *sna* expression. We believe that the key agent of this all or no bistable expression of Snail is the antirepression of competitive ectodermal repressors (Hemavathy et al., 1997). This indirect mechanism of Snail autoregulation may be the basis for producing the unusually sharp border of Snail expression at the boundary between the mesoderm and neurogenic ectoderm. This border determines whether cells become fully committed to EMT at gastrulation. Delays in coordinate *sna* expression are amplified by the dorsal-ventral patterning network to produce bistable gaps in the ventral furrow, particularly in anterior regions where there are slightly diminished levels of Dorsal nuclear transport.

Spectrum of Pausing and Cell Fate Decisions

Our results indicate that the continuum of Pol II pausing seen for different promoters leads to a continuum of temporal coordination in gene activation, spanning from highly stochastic to synchronous. As discussed above, synchronous activation of transcription is essential for coordinating mesoderm invagination; however, the stochastic regulation of gene expression is sometimes used to provide flexibility in cell fate specification within a tissue (Eldar and Elowitz, 2010; Losick and Desplan, 2008). For example, stochastic specification mechanisms underlie fate decisions in the *Drosophila* eye and human immune system (Duffy et al., 2012; Losick and Desplan, 2008), whereby cells must adopt alternate fates to achieve a distribution of distinct functions. For example, there is a 70:30 distribution of alternative ommatidial identities in the eyes of higher Diptera that has been conserved for ~120 MYA (Losick and Desplan, 2008). Similarly, flexibility in the behavior of B lymphocytes is important for immune regulation (Duffy et al., 2012). Modulating the levels of paused Pol II could help tune the proportion of cells that adopt different fates through such stochastic specification mechanisms.

In summary, we have presented evidence that the promoter is a key agent for coordinating gene expression in the different cells of an embryonic tissue. Minimal promoter sequences are sufficient to establish paused Pol II and mediate synchronous patterns of gene expression. There is a tight correlation among the levels of paused Pol II, the time to synchrony, and the coordination of mesoderm invagination. We therefore propose that promoters ensure exquisite control of the complex cellular processes underlying morphogenesis.

EXPERIMENTAL PROCEDURES

Fly Genetics

The following fly lines were used for this study: Sna (Bl3078), NelfE (Bl1569), Spt5 (Bl8352), Trl (Trl^{R67}), and landing site line "VK33" (Bl 24871). *Toll10b* is a maternal dominant gain-of-function mutation (Schneider et al., 1991); transgenes were introduced through the males. The genetic procedure used for the *sna* BAC rescue experiments was performed as described previously by Perry et al. (2010). For more details, see information in the Extended Experimental Procedures.

Recombineering, Cloning, and Transgenesis

BAC recombineering was performed as described previously by Venken et al. (2006). The following CHORI BACs were used: *tup* BAC (84.8 kb, shortened to 60 kb) (CH321-68I16); and *sna* BAC (CH322-18I14-1). Sources of plasmid used and fly transgenesis using targeted integration are described in the Extended Experimental Procedures and Table S3.

FISH and Quantitative Imaging Methods

FISH experiments were performed as described in Bothma et al. (2011). Embryos were imaged on a Carl Zeiss LSM 700 laser-scanning microscope, equipped with a motorized stage. Images were computationally segmented to localize nuclei and nascent transcripts of mRNA. More extensive details on the image analysis are included in the Extended Experimental Procedures.

In order to measure the time to synchrony, activation curves were generated by quantifying the number of nuclei exhibiting nascent transcripts for various embryos at various time points during cc14. By fitting a cumulative gamma distribution, the t50 parameter was evaluated. Detailed description of this assay is provided in the Extended Experimental Procedures.

Pol II ChIP-Seq

Pol II ChIP has been performed as described in Zeitlinger et al. (2007) using a Pol II antibody (CTD4H8; Millipore). Methods employed for library generation and ChIP-seq analysis are detailed in the Extended Experimental Procedures.

Modeling

A detailed description of the mathematical model used to predict the evolution of the Snail protein is provided in the Extended Experimental Procedures. Briefly, ordinary differential equations were used with the following key parameters: the timing of Snail activation, the concentration of a repressor and that of an activator (Dorsal), the number of nearest neighbors, and the diffusion between nuclei.

ACCESSION NUMBERS

All data have been submitted to the GEO under the accession number GSE36310.

SUPPLEMENTAL INFORMATION

Supplemental Information includes Extended Experimental Procedures, seven figures, and three tables and can be found with this article online at http://dx.doi.org/10.1016/j.cell.2013.04.045.

ACKNOWLEDGMENTS

The authors are grateful to Alistair Boettiger for sharing his ideas about Snail autoregulation. We also thank Mike Perry and Valerie Hilgers for their insightful discussions, Didier Rocancourt for help with artwork, and Lily Mirels and Eileen Wagner for comments on the manuscript. M.L. is the recipient of a Human Frontier fellowship. This work was funded by grants from the NIH, GM46638 to M.S.L. and GM47477 to D.S.G. M.L. and J.P.B. initiated efforts to create a stochastic pattern of *snail* activation. They also worked closely to determine activation profiles of both endogenous genes and transgenes containing minimal promoter sequences. J.P.B. conceived the use of *esg* as a means for identifying *sna*$^{-}$/*sna*$^{-}$ mutant embryos. M.L. worked with L.S. and D.S.G. to document the sufficiency of minimal promoter sequences in establishing paused RNA polymerase II via permanganate protection assays. She also worked with E.E., K.C., J.J., and J.Z. to document the spectrum of Pol II binding at different promoters via whole-genome ChIP-seq assays. J.P.B. performed the imaging and developed the segmentation algorithms needed to determine t50 activation profiles. He also performed imaging to count mRNAs and analyzed the models exploring the relationship between timing and levels of gene expression. J.P.B. modeled the dynamics of Snail protein expression. M.L. and E.E. designed and created minigenes and BAC transgenes. M.L. performed the genetic crosses. C.T. injected all the plasmid transgenes, and BestGene injected all the BAC transgenes. S.N. helped M.L. and J.P.B. to collect and stain embryos. M.L., J.P.B., and M.S.L wrote the manuscript.

Received: October 4, 2012
Revised: February 23, 2013
Accepted: April 22, 2013
Published: May 23, 2013

REFERENCES

Adelman, K., and Lis, J.T. (2012). Promoter-proximal pausing of RNA polymerase II: emerging roles in metazoans. Nat. Rev. Genet. *13*, 720–731.

Ashe, H.L., Mannervik, M., and Levine, M. (2000). Dpp signaling thresholds in the dorsal ectoderm of the *Drosophila* embryo. Development *127*, 3305–3312.

Balaskas, N., Ribeiro, A., Panovska, J., Dessaud, E., Sasai, N., Page, K.M., Briscoe, J., and Ribes, V. (2012). Gene regulatory logic for reading the Sonic Hedgehog signaling gradient in the vertebrate neural tube. Cell *148*, 273–284.

Boehm, A.K., Saunders, A., Werner, J., and Lis, J.T. (2003). Transcription factor and polymerase recruitment, modification, and movement on dhsp70 in vivo in the minutes following heat shock. Mol. Cell. Biol. *23*, 7628–7637.

Boettiger, A.N., and Levine, M. (2009). Synchronous and stochastic patterns of gene activation in the *Drosophila* embryo. Science *325*, 471–473.

Boettiger, A.N., and Levine, M. (2013). Rapid transcription fosters coordinate snail expression in the *Drosophila* embryo. Cell Rep *3*, 8–15.

Bothma, J.P., Magliocco, J., and Levine, M. (2011). The snail repressor inhibits release, not elongation, of paused Pol II in the *Drosophila* embryo. Curr. Biol. *21*, 1571–1577.

Chen, H., Xu, Z., Mei, C., Yu, D., and Small, S. (2012). A system of repressor gradients spatially organizes the boundaries of Bicoid-dependent target genes. Cell *149*, 618–629.

Duffy, K.R., Wellard, C.J., Markham, J.F., Zhou, J.H., Holmberg, R., Hawkins, E.D., Hasbold, J., Dowling, M.R., and Hodgkin, P.D. (2012). Activation-induced B cell fates are selected by intracellular stochastic competition. Science *335*, 338–341.

Dunipace, L., Ozdemir, A., and Stathopoulos, A. (2011). Complex interactions between cis-regulatory modules in native conformation are critical for *Drosophila* snail expression. Development *138*, 4075–4084.

Eldar, A., and Elowitz, M.B. (2010). Functional roles for noise in genetic circuits. Nature *467*, 167–173.

Fay, A., Misulovin, Z., Li, J., Schaaf, C.A., Gause, M., Gilmour, D.S., and Dorsett, D. (2011). Cohesin selectively binds and regulates genes with paused RNA polymerase. Curr. Biol. *21*, 1624–1634.

Gaertner, B., Johnston, J., Chen, K., Wallaschek, N., Paulson, A., Garruss, A.S., Gaudenz, K., De Kumar, B., Krumlauf, R., and Zeitlinger, J. (2012). Poised RNA polymerase II changes over developmental time and prepares genes for future expression. Cell Rep. *2*, 1670–1683.

Gilchrist, D.A., Dos Santos, G., Fargo, D.C., Xie, B., Gao, Y., Li, L., and Adelman, K. (2010). Pausing of RNA polymerase II disrupts DNA-specified nucleosome organization to enable precise gene regulation. Cell *143*, 540–551.

Gilchrist, D.A., Fromm, G., dos Santos, G., Pham, L.N., McDaniel, I.E., Burkholder, A., Fargo, D.C., and Adelman, K. (2012). Regulating the regulators: the pervasive effects of Pol II pausing on stimulus-responsive gene networks. Genes Dev. *26*, 933–944.

Guenther, M.G., and Young, R.A. (2012). Grounded: transcriptional pausing in naive mESCs. Cell Stem Cell *10*, 484–485.

Hemavathy, K., Meng, X., and Ip, Y.T. (1997). Differential regulation of gastrulation and neuroectodermal gene expression by Snail in the *Drosophila* embryo. Development *124*, 3683–3691.

Hendrix, D.A., Hong, J.W., Zeitlinger, J., Rokhsar, D.S., and Levine, M.S. (2008). Promoter elements associated with RNA Pol II stalling in the *Drosophila* embryo. Proc. Natl. Acad. Sci. USA *105*, 7762–7767.

Juven-Gershon, T., and Kadonaga, J.T. (2010). Regulation of gene expression via the core promoter and the basal transcriptional machinery. Dev. Biol. *339*, 225–229.

Kalmar, T., Lim, C., Hayward, P., Muñoz-Descalzo, S., Nichols, J., Garcia-Ojalvo, J., and Martinez Arias, A. (2009). Regulated fluctuations in nanog expression mediate cell fate decisions in embryonic stem cells. PLoS Biol. *7*, e1000149.

Kanodia, J.S., Rikhy, R., Kim, Y., Lund, V.K., DeLotto, R., Lippincott-Schwartz, J., and Shvartsman, S.Y. (2009). Dynamics of the Dorsal morphogen gradient. Proc. Natl. Acad. Sci. USA *106*, 21707–21712.

Kanodia, J.S., Kim, Y., Tomer, R., Khan, Z., Chung, K., Storey, J.D., Lu, H., Keller, P.J., and Shvartsman, S.Y. (2011). A computational statistics approach for estimating the spatial range of morphogen gradients. Development *138*, 4867–4874.

Kosman, D., Ip, Y.T., Levine, M., and Arora, K. (1991). Establishment of the mesoderm-neuroectoderm boundary in the *Drosophila* embryo. Science *254*, 118–122.

Lee, H., Kraus, K.W., Wolfner, M.F., and Lis, J.T. (1992). DNA sequence requirements for generating paused polymerase at the start of hsp70. Genes Dev. *6*, 284–295.

Lee, C., Li, X., Hechmer, A., Eisen, M., Biggin, M.D., Venters, B.J., Jiang, C., Li, J., Pugh, B.F., and Gilmour, D.S. (2008). NELF and GAGA factor are linked to promoter-proximal pausing at many genes in *Drosophila*. Mol. Cell. Biol. *28*, 3290–3300.

Leptin, M. (2005). Gastrulation movements: the logic and the nuts and bolts. Dev. Cell *8*, 305–320.

Levine, M. (2011). Paused RNA polymerase II as a developmental checkpoint. Cell *145*, 502–511.

Leptin, M., and Grunewald, B. (1990). Cell shape changes during gastrulation in *Drosophila*. Development *110*, 73–84.

Li, J., and Gilmour, D.S. (2011). Promoter proximal pausing and the control of gene expression. Curr. Opin. Genet. Dev. *21*, 231–235.

Liberman, L.M., Reeves, G.T., and Stathopoulos, A. (2009). Quantitative imaging of the Dorsal nuclear gradient reveals limitations to threshold-dependent patterning in *Drosophila*. Proc. Natl. Acad. Sci. USA *106*, 22317–22322.

Lin, C., Garrett, A.S., De Kumar, B., Smith, E.R., Gogol, M., Seidel, C., Krumlauf, R., and Shilatifard, A. (2011). Dynamic transcriptional events in embryonic stem cells mediated by the super elongation complex (SEC). Genes Dev. *25*, 1486–1498.

Losick, R., and Desplan, C. (2008). Stochasticity and cell fate. Science *320*, 65–68.

Morachis, J.M., Murawsky, C.M., and Emerson, B.M. (2010). Regulation of the p53 transcriptional response by structurally diverse core promoters. Genes Dev. *24*, 135–147.

Nichols, J., and Smith, A. (2011). The origin and identity of embryonic stem cells. Development *138*, 3–8.

Ong, C.T., and Corces, V.G. (2011). Enhancer function: new insights into the regulation of tissue-specific gene expression. Nat. Rev. Genet. *12*, 283–293.

Perry, M.W., Boettiger, A.N., Bothma, J.P., and Levine, M. (2010). Shadow enhancers foster robustness of *Drosophila* gastrulation. Curr. Biol. *20*, 1562–1567.

Reeves, G.T., Trisnadi, N., Truong, T.V., Nahmad, M., Katz, S., and Stathopoulos, A. (2012). Dorsal-ventral gene expression in the *Drosophila* embryo reflects the dynamics and precision of the dorsal nuclear gradient. Dev. Cell *22*, 544–557.

Rushlow, C.A., and Shvartsman, S.Y. (2012). Temporal dynamics, spatial range, and transcriptional interpretation of the Dorsal morphogen gradient. Curr. Opin. Genet. Dev. *22*, 542–546.

Saga, Y. (2012). The synchrony and cyclicity of developmental events. Cold Spring Harb. Perspect. Biol. *4*, a008201.

Schneider, D.S., Hudson, K.L., Lin, T.Y., and Anderson, K.V. (1991). Dominant and recessive mutations define functional domains of Toll, a transmembrane protein required for dorsal-ventral polarity in the *Drosophila* embryo. Genes Dev. *5*, 797–807.

Schuettengruber, B., Ganapathi, M., Leblanc, B., Portoso, M., Jaschek, R., Tolhuis, B., van Lohuizen, M., Tanay, A., and Cavalli, G. (2009). Functional anatomy of polycomb and trithorax chromatin landscapes in *Drosophila* embryos. PLoS Biol. *7*, e13.

Shopland, L.S., Hirayoshi, K., Fernandes, M., and Lis, J.T. (1995). HSF access to heat shock elements in vivo depends critically on promoter architecture defined by GAGA factor, TFIID, and RNA polymerase II binding sites. Genes Dev. *9*, 2756–2769.

Sweeton, D., Parks, S., Costa, M., and Wieschaus, E. (1991). Gastrulation in *Drosophila*: the formation of the ventral furrow and posterior midgut invaginations. Development *112*, 775–789.

Venken, K.J., He, Y., Hoskins, R.A., and Bellen, H.J. (2006). P[acman]: a BAC transgenic platform for targeted insertion of large DNA fragments in *D. melanogaster*. Science *314*, 1747–1751.

Vincent, S.D., and Buckingham, M.E. (2010). How to make a heart: the origin and regulation of cardiac progenitor cells. Curr. Top. Dev. Biol. *90*, 1–41.

Zeitlinger, J., Stark, A., Kellis, M., Hong, J.W., Nechaev, S., Adelman, K., Levine, M., and Young, R.A. (2007). RNA polymerase stalling at developmental control genes in the *Drosophila melanogaster* embryo. Nat. Genet. *39*, 1512–1516.

Cell

EXTENDED EXPERIMENTAL PROCEDURES

Fly Genetics

The *snail* deficiency used in this study also removes some neighboring genes (Bl 3078). In addition to genotyping the embryos with a lacZ from a labeled balancer (hb-lacZ), we use a probe for the *escargo* (*esg*) gene, which next to *snail* and is expressed during cc14 in the ventral ectoderm. The *snail* deficiency we used also deletes this *escargo* gene, but the latter is not present in the 25kb *snail* BAC used in this study.

Recombineering, Cloning, and Transgenesis

Plasmid constructs containing various enhancers (*pannier* enhancer, *sog* enhancer and *snail* shadow enhancer) and promoters (*pnr*, *tup*, *sna*, *sog*, *ths*, *Hsp70*) were built using the pbPHi backbone vector (Venken et al., 2006). Primers used for construct building and recombineering are listed in Table S3. All plasmids and BACs were integrated in the same landing site on chromosome 3 (VK33). The 5′RACE PCR has been performed using the kit firstChoice RLM-RACE from Ambion. The reverse transcription has been performed on RNA collected from 2-4h yw embryos.

Permanganate Genomic Footprinting

Permanganate footprinting on embryos was carried as described in (Ghosh et al., 2011), by adapting the volumes to small amount of DNA. LM-PCR reactions were performed as preciously described (Gilmour and Fan, 2009). All reactions started with 100ng of piperdine-cleaved DNA. The primers used are listed in Table S3. ''Naked DNA'' stands for genomic DNA. The time of permanganate treatment is indicated in Figure 2.

Pol II ChIP

Chromatin immunoprecipitations (ChIP) from approximately 1g of Toll10b, *Pnre-tup*Pr-Y; gd7, TwiBac-*Pnr*Pr-Y or gd7, TwiBac-Y mutant embryos were performed as described in (Zeitlinger et al., 2007). A monoclonal antibody recognizing both the phosphorylated and the nonphosphorylated form of Pol II was used (CTD4H8, Millipore). Sequencing libraries were prepared from 10ng of immunoprecipitated DNA and 50ng input DNA following the Illumina's instructions. The primers used for ChIP-qPCR are listed in Table S3.

ChIP-Seq Analysis

Paired-end sequenced reads for both the RNA Pol II ChIP and the whole-cell extract input control were aligned to the *Drosophila* reference genome (UCSC version dm3) with the addition of a pseudo-chromosome containing the sequence of the synthetic promoter and yellow gene from the BAC insert. Reads were uniquely aligned using Bowtie version 0.12.7 with the following parameters: -X 300 –k 1 –m 1 –l 51 –n 3. Successfully aligned paired reads were merged into single fragments and used to calculate read-count-normalized coverage over the entire genome.

FISH and Immunostaining

Yellow white and transgenic embryos were developed at room temperature and were collected at 1-4 hr of development and were fixed as described in (Kosman et al., 2004). We used the in situ hybridization protocol from (Kosman et al., 2004) with minor modifications. No Proteinase K was used and signal was not amplified using Tyramide amplification. All probes were made with either digoxigenin, biotin or dinitrophenyl conjugated haptens. The primary antibodies used to detect probes were sheep anti-digoxigenin, mouse anti-biotin and rabbit anti-dinitrophenyl (Roche Applied Sciences, Invitrogen). These were labeled with Alexa dyes using Alexa Fluor 555-donkey-anti-sheep, Alexa Fluor 488 donkey-anti-mouse and Alexa Fluor 647 donkey-anti-rabbit secondary antibodies (Invitrogen, Molecular Probes). Nuclei were counter-stained with either DAPI (Invitrogen) or DRAQ5 (Biostatus). All the embryos used for the initiation curves were co-stained with a probe labeling *sog* nascent transcripts. *Sog* has a distinctive expression pattern that allows unambiguous identification of the dorso-ventral orientation of embryos during cc13 and 14. The primers that were used to amplify the DNA fragments that were used to make the different RNA probes are listed in Table S3. We used a guinea-pig antibody anti-snail, a rat antibody anti-twist and a rabbit anti-ß-galactosidase. The twi and sna antibodies were kindly provided by Dr. Wieschaus (Princeton).

Confocal Imaging

Embryos were imaged on a Carl Zeiss LSM 700 Laser Scanning microscope, equipped with a motorized stage. For embryos used to examine activation kinetics 20-25 section z-stacks through the nuclear layer at 1/2 micron intervals were taken using a Plan-Apochromat 20x/0.8, WD = 0.55 mm lens. They were taken at 2048x2048 resolution with 8 bit color depth. Embryos were roughly staged by quantitative analysis of nuclear density and by developmental morphology. We examined embryos from the beginning of cell cycle 13 through to the onset of cephalic furrow formation. For the initiation curves acquired during cc13 and cc14 all the embryos on a slide that were in the appropriate orientation to see the expression pattern of the enhancer of interest were imaged (i.e., dorsal view for the *pnr* enhancer constructs and ventral view for the *sna*il enhancer constructs). The orientation was judged by examining the expression pattern of *sog* nascent mRNA which was placed in a different channel to that of the transgene.

For the images acquired for the mRNA counting 50 section z-stacks through the outer layer of cells at 1/3 micron intervals were taken using a Plan-Apochromat 63x/1.40 oil lens. They were taken at 2048x2048 resolution at 16 bit color depth.

Image Analysis for Determining Fraction Active Nuclei

We wrote an automated image segmentation program in MatlabR2011 (MathWorks) to identify and count all stained nuclei and detect foci of nascent transcription. This was then used to determine what fraction of nuclei in a region of gene expression was active for many different embryos.

For the image stack containing the DNA counter stain, Z-stacks were projected into two-dimensional images by selecting the maximum intensity pixel in each stack. For the channels that contained the signal from the in situ probes each image plane was filtered by a Laplacian of Gaussian and then the stack was max projected to a two dimensional image. The core of each individual nucleus was determined using the DNA counter-stain, processed with a Laplacian of Gaussian filter, which allows robust determination of nuclei using blob detection, size selection, and signal strength to inform classification. This was followed by an object dilation algorithm to create a computational mask in which all pixels in an embryo are assigned to a uniquely identified nucleus.

The script then determines the transcriptional activity of nuclei by identifying which in situ signals from nascent mRNA are present in the region assigned to different nuclei. True hybridization foci or dots are identified through a series of filtering steps and segmentation. The 2D projection is filtered by a Laplacian of Gaussian filter which is then segmented using a combination of a watershed algorithm (to split dots that are joined) and intensity based thresholding.

To address possible misclassification due to uncertainty in determining the nuclear boundary, transcripts localized to pixels adjacent to the nuclear boundary may be automatically reassigned to the neighboring nucleus if the original parent nucleus already contains an interior localized probe. This exploits the fact that the hetero or homo allelic expression of the reporter should result in no more than one or two foci per nucleus, respectively. An iterative extension of this algorithm also insured reliable classification when several adjacent nuclei each had transcripts that localized to boundary pixels.

To determine the fraction of inducible nuclei that are actively expressing a particular gene/enhancer, the subset of cells that make up the expression pattern needs to be defined. The enhancers used in this study are heavily studied and therefore the exact locations where they drive expression are well characterized. This allows the software user to manually select the region of expression based on the percentage of the embryo and spatial profile of other genes that serve as fiduciary markers. For our analysis we focus on a subset of the expression pattern that we define as the ''core'' region of expression. The core region of expression satisfies the following two criteria. First, nuclei are activated with no significant spatial bias in this region. Second, the expression pattern displays no spatial dynamics across cc14. For example the expression of *snail* is refined at the poles of the embryo during cc14 and so nuclei within 15%EL of the poles were not included in the core region for analysis of constructs with the *snail* enhancer. We specifically focused on the core of the pattern to avoid convoluting the dynamics of changes in the expression pattern of the gene with that of gene activation. The core region consists of many hundreds of nuclei and using this we can calculate the fraction of core pattern ''on''. This is done for many embryos and forms the basis for determining the kinetics of activation described in later sections.

Quantifying Initiation Dynamics and Determining t50

To quantify the initiation dynamics, we combined the calculated fraction ''on'' for all the ~50-100 embryos for the different constructs tested. The embryo collections were designed to ensure that embryos are distributed in an unbiased way across the entirety of the one hour window of cc14. Under the assumption that the fraction of the core pattern active increases monotonically with time (which was verified by examining the fraction of pattern ''on'' at different stages of membrane invagination), we can order these embryos from youngest to oldest based on the fraction of pattern that is active. This means that we know the relative age of each embryo but don't know the absolute age. To determine the kinetics, we can assume that the timing between embryos is uniform at the cost of introducing uncertainty in the activation kinetics. We measure large numbers of embryos and so we sample the period of interest densely and as a result, the uncertainty introduced with this method is relatively small. We can explicitly calculate the uncertainty introduced using our model to describe the timing of gene activation. The uncertainty in time introduced with this method is less than 5 min in most cases (see Table1, Figure S1, and Table S1), which is sufficient for our purposes and significantly better than what can be obtained by monitoring membrane invagination.

In order to better understand the process of gene activation and be able to compare activation kinetics across different constructs and promoters, we needed to develop a model to characterize the time to gene activation. From what we have measured, it is clear that the time it takes for a particular nucleus to start transcribing a gene is a random variable. Exactly how pausing will affect the stochastic molecular processes that set the timescale for the activation of gene expression are not understood. Hence, it would be very difficult to derive a distribution with few free parameters from a minimal mechanistic model. Following the principle of maximum entropy, we decided that the most appropriate distribution to use to model the time to activation would be the gamma distribution (Hogg and Craig, 1978).

The gamma distribution is widely used to model stochastic waiting times in a range of other contexts and has only two free parameters (Friedman et al., 2006) (Hogg and Craig, 1978). If the time to activation in a given nucleus is described by a gamma distribution, then the fraction of the pattern ''on'' at a given time is given by the gamma cumulative distribution function (GCDF). We were encouraged to find that even with just 2 free parameters, the GCDF was able to fit the activation curves we measured for the myriad of different promoter and enhancer combinations very well (see Figures S1A and S1B). Based on these fitted curves (which took the

entire data set into account), we determined a parameter to characterize how quickly genes were activated. We calculated what we refer to as the t50, which is the expected time at which half of the nuclei in the core of a pattern are activated (see Figures S1A and S1B). With this model, we can computationally choose random embryos and then construct kinetic curves by ordering them (Figure S1C). Figure S1C shows that even with multiple different sampling, the generated activation curve is very similar to the original data and the fitted curve. We can go through this process of simulating activation profiles many hundreds of times and fit a GCDF to each of the computational curves generated this way (see Table S1 for fit parameters). By comparing the different curves to each other, we can determine the uncertainty in the timing associated with a particular fraction of the pattern on and t50 specifically (Figure S1D). Since the simulations explicitly take into account the number of embryos used and the profile of the activation for each different experiment, we can obtain an uncertainty value unique to each set of data. This analysis shows that for almost all of the constructs this is less than 5 min (Table1).

Analysis for mRNA Counting

Single molecule FISH was performed as described in (Boettiger and Levine, 2013).

Determining Promoter Strength

We determine the relative strength of the *pnr*, *ths* and *sna* promoters by combining our data, i.e., measured levels of the *yellow* reporter mRNA and promoter activation kinetics with a model describing how the amount of mRNA in a cell changes with time. This model has two parameters: the rate at which the promoter produces mRNA once activated, i.e., the promoter strength, and the degradation rate of this mRNA. Our measurements alone do not allow us to independently specify both parameters. However by combining the known *sna* promoter strength (Boettiger and Levine, 2013) with our data, we can determine the half-life of the *yellow* reporter mRNA. Fortunately, the reporter mRNA is the same for all constructs. Using this method (detailed below; Figures S4E–S4I) we determine the relative promoter strength of the different promoters is 1, 0.93 ± 0.15 and 0.47 ± 0.10 for *sna*, *ths* and *pnr*, respectively.

The model we use assumes that once a locus starts transcribing mRNA it produces mRNA at a constant rate, which depends on the intrinsic strength of the promoter, α. The fraction of loci in the core region that are transcribing at a given time is approximated by the measured activation curve defined by A(t). The history of promoter activity, i.e., how recently the promoter entered an actively transcribing state in a given nucleus can have a significant impact on the amount of mRNA present before steady state is reached. The other parameter is the degradation rate of the mRNA, λ. Under these assumptions it is possible to formulate an ordinary differential equation (ode) that describes how the average number of mRNAs per cell, N(t), change as a function of time, t:

$$\frac{dN(t)}{dt} = \alpha \times A(t) - \lambda \times N(t).$$

This ode can then be solved numerically.

Early estimates of promoter strength in *Drosophila* vary from about 1 mRNA/minute per template for histone genes (Anderson and Lengyel, 1980) to 10 mRNAs/minute per template in the case of the heat shock genes (O'Brien and Lis, 1991). The promoter strength for the *sna* promoter has recently been measured to be 6 mRNAs/minute (Boettiger and Levine, 2013).

The half-life for mRNA in the *Drosophila* embryos has also been measured for ftz to be between 6-10 min (Edgar et al., 1986). The half-life of *snail* mRNA has been measured to be ~15 min (Boettiger and Levine, 2013). Many mRNAs expressed in the early embryo are likely to have similarly half-lives around 5 −15 min since mRNA expression patterns change on this timescale and mRNA accumulation has been shown to closely follow that of the transcription. Figure S4H shows the calculated number of *yellow* mRNAs at the onset of gastrulation for the *sna* promoter construct and how this varies as a function of promoter strength and mRNA half-life. By using the known *sna* promoter strength (6 mRNAs/minute), the measured number of *yellow* mRNAs (100 ± 30 mRNAs/cell) for this construct and the calculated number of *yellow* mRNAs from the model we can back out an estimate for the *yellow* mRNA half-life of 6 ± 1 min.

By using the promoter activation curve measured for the construct with the *ths* promoter, we can estimate the number of *yellow* mRNAs at the onset of gastrulation and how this varies as a function of promoter strength and mRNA half-life (Figure S4I). Since the mRNA half-life is 6 ± 1 min and the number of *yellow* mRNAs is 60 ± 20, we can determine the strength of the *ths* promoter. This yields a value for the *ths* promoter, which is 5.6 ± 1 mRNAs/min and so relative to the strength of the *snail* promoter 0.93 ± 0.15. This shows that the *ths* and *sna* promoters have very similar promoter strengths in spite of showing different initiation kinetics.

We can similarly calculate the promoter strength for the *pnr* promoter construct (Figure S4I) (mRNA half-life of 6 ± 1 min; number of *yellow* mRNAs which is 30 ± 10). This yields a value for the *pnr* promoter, which is 2.8 ± 0.6 and so relative to the strength of the *snail* promoter 0.47 ± 0.10. This shows that the *ths* and *pnr* promoters have very different promoter strengths, in spite of showing very similar initiation kinetics.

Modeling Evolution of Snail Protein

Overview

In order to understand the phenotypes we observed when we changed promoters we developed a model to describe the evolution of the Snail protein expression pattern in the early embryo. We sought to simplify the system as much as possible while keeping it

realistic enough to incorporate the wealth of quantitative information available in the early *Drosophila* embryo (Fowlkes et al., 2008) (Alon, 2006). For example, the spatial profile and dynamic behavior of the Dorsal gradient that specifies Snail has been well characterized recently (Reeves et al., 2012);(Kanodia et al., 2009, 2011). Estimates are also available for the timescales of diffusion, protein synthesis and protein half-lives and molecular binding constants (Gregor et al., 2007a; Gregor et al., 2007b; Jaeger et al., 2004; Lehmann and Nüsslein-Volhard, 1987); (Zhao et al., 2002); (Ma et al., 1996); (Daniels et al., 2012). Our goal was to see what would happen when you perturb the timing and coordination of Snail transcriptional activation in the context of a model based on what is known about the early embryo and some reasonable estimates for parameters that are not known. We do not claim that our model is completely comprehensive; rather it serves as a tool to judge how differences in kinetics of coordination may lead to changes in the Snail expression pattern and then coordination of morphogenesis.

We represent the embryo as a two dimensional grid of nuclei. The nuclear grid used for the modeling was obtained by segmenting a fluorescent confocal stack of a cc14 embryo (Figure 6). This yields a pseudohexagonal grid consisting of about ~2000 nuclei where the location and connectivity of all the nuclei are known. In our model each of these nuclei are considered a unit. The evolution of the concentration of Snail in an individual nucleus is described by a differential equation. This differential equation has terms that describe synthesis rates that depend on the regulatory network, first order decay and diffusion between neighboring nuclei (see below).

The different kinetics of activation for the different promoters is included in the evolution of the model as follows. We assume that there is a delay between the start of cc14 and when each nucleus can starts producing protein. This delay is modeled as a random variable that follows a gamma distribution and the parameters that define this distribution are different for different promoters. In the model we assume that to a good approximation there exists a linear correlation between the amount of snail mRNA and protein. This has been illustrated in the literature (McHale et al., 2011) and may be due to the short half-lives of both mRNA and protein in the early *Drosophila* embryo (Jaeger et al., 2004). We use the t50 value defined earlier to characterize the different timing of activation for the different constructs. All other parameters are kept the same. How the Snail concentration changes with time in each nucleus can then be obtained by numerically solving the differential equation given some initial conditions. The next section describes the relevant components of the regulatory network.

Regulatory Network

Dorsal

The key morphogen that patterns the dorso-ventral axis of the *Drosophila* embryo is the transcription factor Dorsal (Stathopoulos and Levine, 2004). The nuclear concentration of the Dorsal protein forms a gradient that is high in ventral nuclei and low in dorsal regions. The spatial profile of this gradient has been well characterized by a number of groups and has been shown to follow a Gaussian function (Reeves et al., 2012);(Kanodia et al., 2009, 2011). Through a combination of modeling and experiments it has also been shown that the Dorsal gradient is dynamic. At a given anterior-position position the shape and width of the gradient is static but the amplitude increases with time (Reeves et al., 2012; Kanodia et al., 2009; Liberman et al., 2009). It has also been shown that the width of the gradient changes significantly along the anterior posterior axis as shown in Figures S6A–S6C (Kanodia et al., 2009). There has been some disagreement over the exact width of the gradient, but this is largely a result of different groups measuring the profile of the gradient at different anterior-posterior positions along the embryo in earlier studies. Due to the careful characterization of the spatial and temporal profile of the gradient we can build both of these features into our model to predict the evolution of the Snail expression pattern.

Snail

Through a combination of classic enhancer mutagenesis experiments it was shown that Dorsal acts as an activator that specifies the domain of Snail expression through a standard affinity threshold model (Ip et al., 1992). It activates transcription in concert with another transcriptional activator Twist whose expression pattern is also defined by Dorsal. Twist plays a permissive role in the specification of Snail and because it follows Dorsal we have not explicitly included it in our model. Instead we assume that considering Dorsal as the major activator captures most of the important aspects of activation. Hence according to what is known about the specification of Snail so long as the Dorsal and Twist gradients are intact the domain of Snail specification should remain unchanged.

There has however been circumstantial evidence that Snail may play a role in defining its own expression pattern (Hemavathy et al., 1997). Embryos that are homozygous for the strongest *snail* loss of function allele show normal patterns of *snail* mRNA during cc13 but that mRNA is lost in the presumptive mesoderm during cc14. The Snail[18] allele produces mRNA and protein but the lesion was not characterized (Hemavathy et al., 1997). To better understand the role that Snail is playing in shaping its own mRNA expression we looked at reporter expression driven by snail enhancers in embryos where there is no snail protein. We used a ~25kb reporter BAC which contains all of the known snail regulatory sequences relevant for early expression where the snail coding region has been replaced with that of the yellow reporter (Perry et al., 2010). We looked at the expression of this reporter BAC in embryos that were homozygous for a snail deficiency. Using this approach we saw clear evidence for snail auto regulation during the course of cc14 (Figures S5G–S5J). At the onset of cc 14 the expression of yellow nascent dots looks to that of a control embryo where there is snail present. However at the end of cc14 the reporter expression is severely compromised and absent through most of the presumptive mesoderm. This is despite the fact that both Dorsal and Twist expression are normal in these embryos.

The key role that Snail plays in specifying its own expression pattern is also clear from what we observe in the rescue constructs (Figure 5). We observe the complete loss of snail protein and mRNA in variable regions of the presumptive mesoderm. In the rescue

constructs the spatial pattern of snail expression is changed. This is quite different to what we observe for the pattern defined by the reporter genes with the *snail* enhancer (Figure 4). Here nuclei across the whole presumptive mesoderm showed expression. The constructs with different promoters showed different kinetics of filling out the domain but we see no evidence for any spatial difference in the expression pattern.

Mutual Repression

The previous experimental evidence indicates that Snail protein is either directly or indirectly involved in regulating its own expression in a positive way. When snail protein expression is compromised the snail expression pattern is compromised. Snail has been shown to be a potent transcriptional repressor and there is no evidence for it being able to act as a transcriptional activator. However we attempted to model the feedback as direct by enabling snail to activate its own transcription but the simulations from this model were unable to reproduce the phenotypes we observed. Hence it is most likely that snail's positive regulation on itself is mediated indirectly, by having it repress a transcriptional repressor that can repress snail. There is evidence for mutual repression between snail homologs and other ectodermal repressors (Acloque et al., 2011). From the domain of snail expression and the timing of the loss of snail it is most likely that the repressor is of an ectodermal origin and so would be activated by lower threshold concentrations of the Dorsal protein. By invoking such a mutually repressive interaction we were able to explain the dependence of snail transcription on its own expression and by building it into the model we could reproduce the observed patches of snail expression.

Equations and Parameters

In the following section we list all the equations that were used in building the model of the DV gene network to look at the evolution of snail protein. This formalizes the concepts that were discussed in the earlier sections. Not all the parameters that the equations depend on have been measured and so some needed to be estimated from values that are available for similar processes. Moreover the approach with the modeling was not to fully constrain the model based on our observations but rather to see how the model would respond to difference in the coordination of transcription with some reasonable estimates of parameters that are not known. Equations 1 and 2 describe the temporal evolution of the snail (Sna) and repressor (Rep) concentration in the i'th nucleus which has a particular position along the anterior-posterior axis (y_i) and dorso-ventral axis (x_i). All simulations were evolved forward for a period of 60 min representing the time from the onset of cc14 to when the snail pattern stabilizes and the first signs of gastrulation appear.

$$\frac{d[Sna_i]}{dt} = \frac{k_{1i}(x_i, y_i, t)}{\left[\frac{Rep_i}{K_R}\right]^{n_1} + 1} - \lambda_1 [Sna_i] + D(t) \sum_{j=1}^{NN} \frac{[Sna_j - Sna_i]}{NN} \qquad \text{(Equation 1)}$$

$$\frac{d[Rep_i]}{dt} = \frac{k_{2i}(x_i, y_i, t)}{\left[\frac{Sna_i}{K_S}\right]^{n_2} + 1} - \lambda_2 [Rep_i] + D(t) \sum_{j=1}^{NN} \frac{[Rep_j - Rep_i]}{NN} \qquad \text{(Equation 2)}$$

$$D(t) = \begin{cases} D_0 \left[1 - \frac{t}{90}\right], & t \leq 30 \\ \frac{2D_0}{3} \left[1 - \frac{t-30}{30}\right], & 30 < t \leq 60 \end{cases}, \qquad \text{(Equation 3)}$$

where NN is the number of nearest neighbor nuclei. D_0 is the diffusion constant between nuclei and was set to be equal to 3/min (unitless because it's diffusion between nuclei) this number was based on the geometry of nuclei and the value of $\sim$1 μm^2 /s which is measured for the Bcd protein in the early embryo (Gregor et al., 2007a; Gregor et al., 2007b). The strength of diffusion between nuclei was decreased with time during cc14 according to the dynamics of the slow and fast phases of membrane invagination according to Equation 3. The half-lives of transcription factors in the *Drosophila* embryo have been estimated to be between 5 to 30 min (Jaeger et al., 2004). The snail protein domain refines rapidly at the poles when it is repressed during cc 14 and so we reasoned that the half-life would be close to the lower end of this range. A half-life of 7 min was used in our simulations for the half-life of both snail and the repressor. We assumed binding affinities (K_R and K_S) on the order of $\sim$10 nM based on the typical range seen for transcription factors in the early embryo (Jaeger et al., 2004, and references therein). We speculate that there is likely to be some degree of cooperativity in binding and so chose values for n_1 and n_2 to be equal to 5. The role of Dorsal and differing initiation kinetics comes in through the synthesis terms and so these are explicitly defined and explained in the next section.

Equation 4 describes the snail protein synthesis term in the i'th nucleus and how it implicitly depends on space and time. Much of the implicit dependence on space and time comes through the spatial and temporal dependence of the Dorsal gradient itself. The absolute concentration of Dorsal has not been measured but because we know the relative value where the snail boundary occurs when the gradient stabilizes we can estimate the relative K_{Ds} value to be equal to 0.5 (Kanodia et al., 2009). The dependence of the dorsal gradient on space and time will be discussed below. Some degree of cooperativity was assumed and so n_3 was chosen to be 5.

$$k_{1i}(x_i, y_i, t) = \frac{r_s}{\left[\frac{K_{DS}}{Dorsal(x_i, y_i, t)}\right]^{n3} + 1} \times H(t - TA_i) \quad \text{(Equation 4)}$$

$$TA_i \sim \Gamma(a, b) \equiv Gamma(a, b) \quad \text{(Equation 5)}$$

The different promoter kinetics is included in the second half of the term and through Equation 5. The term representing dorsal mediated activation is multiplied by a Heaviside step function that effectively allows protein only to be produced after a given time TA_i. This time is a random variable that follows a gamma distribution characterized by the variables a and b and is the source of the variability seen in our simulations. This is how we incorporate the delay in the onset of transcription into the model that looks at the evolution of the snail protein. For our analysis we fixed a to be equal to one and examined how the behavior of the system changed as b was increased which caused a corresponding increase in the value of t50. We assumed a synthesis rate (r_s) of ~1 nM/min which is well within the realms of what has been estimated for the early embryo (Jaeger et al., 2004, and references therein).

The synthesis term for the repressor is similarly defined except it doesn't have timing of activation component (we assume is comes on quickly). Due to the fact that we consider it to be a neurogenic repressor the sensitivity to dorsal must be significantly higher than snail and so we set the relative K_{Ds} value to be equal to 0.1. The synthesis rate was set to (r_r) 0.3 nM/min. Some degree of cooperativity was assumed and so n_4 was chosen to be 5.

$$k_{2i}(x_i, y_i, t) = \frac{r_r}{\left[\frac{K_{Dr}}{Dorsal(x_i, y_i, t)}\right]^{n4} + 1} \quad \text{(Equation 6)}$$

The final part of the model takes the spatial and temporal profile of the dorsal gradient into account and is shown in Equation 7. The dynamics of the gradient were imaged live recently (Reeves et al., 2012) and this revealed that the values for the parameters B, A and t_D are 0.2, 0.8 and ~5 min, respectively. How the profile of the Dorsal gradient changes as a function of anterior-posterior position was taken from measured data Figure S6, (Kanodia et al., 2009). Nuclei in the core snail domain were initialized with ~1nM of snail protein that was normally distributed with a variance of 0.1 nM. Reducing this variance did not lead to significant differences in the simulation outcomes.

$$Dorsal(x_i, y_i, t) = \left[B + A\left(1 - e^{-t/\tau_D}\right)\right] \times e^{-\frac{x_i^2}{2\sigma(y_i)^2}} \quad \text{(Equation 7)}$$

Model Behavior

When we examined the behavior of the model with the parameter values listed above, we observed four qualitatively distinct classes of behavior as the t50 or time to synchrony was varied. One of the main features that distinguish the four classes is the degree of variability across simulations. This variability is a consequence of the inbuilt random nature of the activation time of individual cells, which depending on the degree of coordination is either suppressed or enhanced as the system evolves.

Class 1 occurs for rapid t50s from 0 to 4 min, class 2 for moderate t50s from 4 to 7 min, class 3 for slow t50s from 7 to 12 min and class 4 for t50s greater than 12 min. When the time to activation is rapid, the behavior of the Snail expression pattern was consistent for many different simulation runs which represent individual embryos. All the simulation runs finished with embryos where the Snail domain specified was completely intact and encompassing the entire presumptive mesoderm (see Figure S6). Class 1 which includes t50 values from 0 to 4 min most closely resembles what we observe for rescues with the *snail* promoter where the domain of Snail expression consistently encompassed the entire mesoderm.

Class 2 is characterized by the onset of variability in the spatial distribution of Snail expression. As t50 is increased, a small proportion of simulations start showing gaps in the snail expression pattern in the anterior region of the embryo (see Figure S6). As t50 is further increased the fraction of embryos showing these gaps grows and simulation runs start to appear where Snail is completely lost in the anterior third of the *Drosophila* embryo (see Figure S6). The variability seen is also sufficiently large that rarely there are simulations that converge to a complete loss of snail expression. Class 2 encompasses t50 values from 4 to 7 min and is most similar to what we observe for rescues with the *sog* promoter.

Class 3 is characterized by the consistent absence of Snail expression in the anterior third of the embryo. In this class simulations that show absolutely no snail expression become much more common and when there the Snail domain is restricted to the posterior regions of the embryo (see Figure S6). Class 3 encompasses t50 values from 7 to 12 min and is most similar to what we observe for the rescue constructs with the *ths* promoter.

Class 4 is characterized by the complete absence of a stable region of snail expression. As t50 is increased beyond 12 min out of hundreds of simulation runs none produce stable regions of snail expression.

Sensitivity Analysis of Key Parameters

The behavior of the model depends on a number of parameters but for simplicity we focus on describing the sensitivity to several of the key parameters, namely the diffusion strength, degree of cooperativity and protein half-life. In examining the behavior of the

model as these parameters were varied, we saw a similar trend: as the parameters are changed the quantitative behavior of the model changes as a function of different activation kinetics, but the qualitative behavior of the model is robust, i.e., the 4 regimes described previously occur for different ranges of t50 values but they nonetheless persist (Figures S6D–S6G and S7).

One of the key parameters in the model is the degree of cooperativity (n). In the simulations we chose a value for the strength of cooperativity of 5 (Figure S7). The qualitative behavior of the model is robust when the degree of cooperativity falls within the range of 3 to 7. When the degree of cooperativity is reduced, the onset in variable Snail expression patterns is shifted to larger values of t50. Specifically when the degree of cooperativity is set to 3, the onset of variable Snail expression patterns occurs at a t50 value of 9 min as compared to 4 min for a degree of cooperativity of 5. This shift is illustrated by comparing Figure S7A, which shows an embryo histogram when t50 is 5.4 min and n = 3, and Figure S6E, which shows an embryo histogram when t50 is 5.4 min and n = 5. For the simulation with the higher cooperativity and equivalent t50, the Snail expression is variable while for the simulation with lower cooperativity there is no significant variability in Snail expression. Figure S7B shows that as the cooperativity is increased, the onset of variable expression occurs for smaller values of t50. When comparing Figure S7B with Figure S6E, one can see that the Snail pattern is far more variable at the same t50 value when the degree of cooperativity is increased from 5 to 7.

The strength of diffusion plays a key role in the model of Snail evolution. As the strength of diffusion is varied the t50 value at which variability in Snail expression starts to occur shifts, but the qualitative behavior remains the same. Figures S6E, S7C, and S7D show that when the strength of diffusion (D) is reduced from 3 to 1, the essentially invariant Snail expression profiles persist for larger values of t50 but Snail expression becomes variable as t50 is further increased. Figures S6E, S7E, and S7F show that when the strength of diffusion is increased from 3 to 6 the Snail expression profiles become variable at smaller values of t50. While the Snail profiles are essentially invariant for a t50 value of 1.7 min when this is increased to 5.4 min, the profiles become highly variable with most simulations failing to have stable Snail expression which is quite different to what is observed when the diffusion strength is 3 for the same t50 value as shown in Figure S6E.

The degradation rate of the Snail protein, which is inversely related to the protein half-life, plays an important role in setting the timescale of model evolution. In the main modeling section we chose a degradation rate of λ_s of 0.1/min. Figures S6D, S7G, and S7H show that as one increases the degradation rate of λ_s to 0.15/min the range of t50 values for which stable snail expression is obtained shifts to smaller t50 values. Specifically, even though the Snail expression domain is essentially invariant for a t50 value of 1.4 min, it becomes significantly more variable as t50 is increased to 2.8 min. Figure S6D shows that when λ_s is equal to 0.1/min, the Snail expression pattern is invariant even when t50 is equal to 3.4 min. Figures S7I and S7J show that as one decreases the degradation rate of λ_s to 0.05/min, the range of t50 values for which stable Snail expression is obtained shifts to larger t50 values. To have a comparable degree of variability in the Snail expression pattern for a λ_s value of 0.15/min at a t50 value of 2.8 min the t50 value needs to be increased to 13.9 min for a λ_s value of 0.05/min.

SUPPLEMENTAL REFERENCES

Acloque, H., Ocaña, O.H., Matheu, A., Rizzoti, K., Wise, C., Lovell-Badge, R., and Nieto, M.A. (2011). Reciprocal repression between Sox3 and snail transcription factors defines embryonic territories at gastrulation. Dev. Cell *21*, 546–558.

Alon, U. (2006). An Introduction to Systems Biology: Design Principles of Biological Circuits (Boca Raton, FL: Chapman & Hall/CRC).

Anderson, K.V., and Lengyel, J.A. (1980). Changing rates of histone mRNA synthesis and turnover in *Drosophila* embryos. Cell *21*, 717–727.

Daniels, B.R., Rikhy, R., Renz, M., Dobrowsky, T.M., and Lippincott-Schwartz, J. (2012). Multiscale diffusion in the mitotic *Drosophila melanogaster* syncytial blastoderm. Proc. Natl. Acad. Sci. USA *109*, 8588–8593.

Edgar, B.A., Weir, M.P., Schubiger, G., and Kornberg, T. (1986). Repression and turnover pattern fushi tarazu RNA in the early *Drosophila* embryo. Cell *47*, 747–754.

Fowlkes, C.C., Hendriks, C.L., Keränen, S.V.E., Weber, G.H., Rübel, O., Huang, M.Y., Chatoor, S., DePace, A.H., Simirenko, L., Henriquez, C., et al. (2008). A quantitative spatiotemporal atlas of gene expression in the *Drosophila* blastoderm. Cell *133*, 364–374.

Friedman, N., Cai, L., and Xie, X.S. (2006). Linking stochastic dynamics to population distribution: an analytical framework of gene expression. Phys. Rev. Lett. *97*, 168302.

Ghosh, S.K., Missra, A., and Gilmour, D.S. (2011). Negative elongation factor accelerates the rate at which heat shock genes are shut off by facilitating dissociation of heat shock factor. Mol. Cell. Biol. *31*, 4232–4243.

Gilmour, D.S., and Fan, R. (2009). Detecting transcriptionally engaged RNA polymerase in eukaryotic cells with permanganate genomic footprinting. Methods *48*, 368–374.

Gregor, T., Tank, D.W., Wieschaus, E.F., and Bialek, W. (2007a). Probing the limits to positional information. Cell *130*, 153–164.

Gregor, T., Wieschaus, E.F., McGregor, A.P., Bialek, W., and Tank, D.W. (2007b). Stability and nuclear dynamics of the bicoid morphogen gradient. Cell *130*, 141–152.

Hogg, R.V., and Craig, A.T. (1978). Introduction to Mathematical Statistics, 4th Edition (New York: Macmillan).

Ip, Y.T., Park, R.E., Kosman, D., Yazdanbakhsh, K., and Levine, M. (1992). dorsal-twist interactions establish snail expression in the presumptive mesoderm of the *Drosophila* embryo. Genes Dev. *6*, 1518–1530.

Jaeger, J., Surkova, S., Blagov, M., Janssens, H., Kosman, D., Kozlov, K.N., Manu, Myasnikova, E., Vanario-Alonso, C.E., Samsonova, M., et al. (2004). Dynamic control of positional information in the early *Drosophila* embryo. Nature *430*, 368–371.

Kosman, D., Mizutani, C.M., Lemons, D., Cox, W.G., McGinnis, W., and Bier, E. (2004). Multiplex detection of RNA expression in *Drosophila* embryos. Science *305*, 846.

Lehmann, R., and Nüsslein-Volhard, C. (1987). hunchback, a gene required for segmentation of an anterior and posterior region of the *Drosophila* embryo. Dev. Biol. *119*, 402–417.

Ma, X., Yuan, D., Diepold, K., Scarborough, T., and Ma, J. (1996). The *Drosophila* morphogenetic protein Bicoid binds DNA cooperatively. Development *122*, 1195–1206.

McHale, P., Mizutani, C.M., Kosman, D., MacKay, D.L., Belu, M., Hermann, A., McGinnis, W., Bier, E., and Hwa, T. (2011). Gene length may contribute to graded transcriptional responses in the *Drosophila* embryo. Dev. Biol. *360*, 230–240.

O'Brien, T., and Lis, J.T. (1991). RNA polymerase II pauses at the 5′ end of the transcriptionally induced *Drosophila* hsp70 gene. Mol. Cell. Biol. *11*, 5285–5290.

Stathopoulos, A., and Levine, M. (2004). Whole-genome analysis of *Drosophila* gastrulation. Curr. Opin. Genet. Dev. *14*, 477–484.

Zhao, C., York, A., Yang, F., Forsthoefel, D.J., Dave, V., Fu, D., Zhang, D., Corado, M.S., Small, S., Seeger, M.A., and Ma, J. (2002). The activity of the *Drosophila* morphogenetic protein Bicoid is inhibited by a domain located outside its homeodomain. Development *129*, 1669–1680.

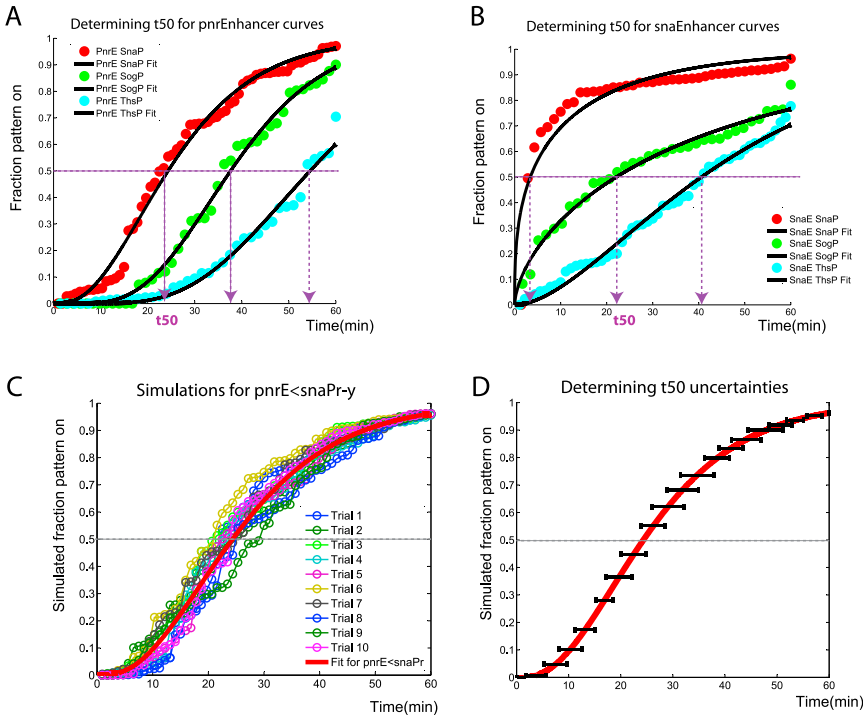

Figure S1. Determining t50 for the Activation Curves, Related to Figure 1 and Table1

(A) Graph showing the ordered fraction of the core pattern that exhibits nascent transcripts for different embryos. The total time of the relevant part of cc 14 is 60 min and so the axis represents this. Three different transgenic lines are represented: *pnrE < snaPr* (red), *pnrE < sogPr* (green) and *pnrE < thsPr* (blue). For each measured curve, we fit a cumulative gamma distribution (see supplementary methods for details), shown in black. From the fitted cumulative gamma function, we determine the t50 value, defined by the time it takes for an embryo to show nascent transcripts in 50% of the core pattern.

(B) Similarly to (A), this graph shows the measured and fitted activation curves to determine the t50 values for transgenic embryos with the *snail* enhancer.

(C) Simulated activation curves plotted with actual curve to illustrate that for large numbers of embryos they compare favorably (see supplementary methods for details).

(D) Graph illustrating how the t50 uncertainties are obtained. The uncertainty is the standard deviation in the difference between the measured t50 and the estimated t50 for hundreds of simulations. All t50s and their estimated uncertainties are summarized in Table1 (see also Table S1).

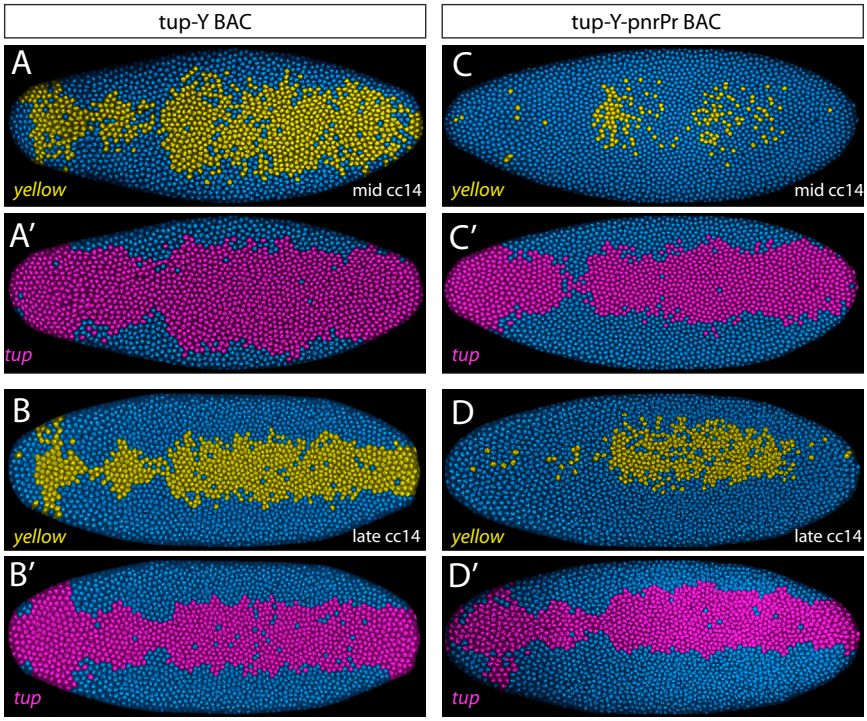

Figure S2. The *pnr* Promoter Is Sufficient to Delay *tup* Expression, Related to Figure 1

Processed images after in situ hybridization of transgenic embryos with intronic probes for the *yellow* reporter gene (BAC transgenes) (shown in yellow) or endogenous *tup* (shown in magenta) in the same embryo.

(A and A′) Reporter (A) and endogenous *tup* expression (A′) in a mid cc14 embryo containing one copy of the *tup*-Y BAC.

(B and B′) Reporter (B) and endogenous *tup* expression (B′) in an embryo just prior to the onset of gastrulation which contains one copy of the *tup*-Y control BAC.

(C and C′) Reporter (C) and endogenous *tup* expression (C′) in a mid cc14 embryo that contains one copy of the *tup*-Y BAC where the *tup* promoter region has been replaced by an equivalent sequence from the *pnr* promoter. Note that expression is significantly perturbed.

(D and D′) Same as in (C) and (C′) except the embryo is older being at the onset of gastrulation.

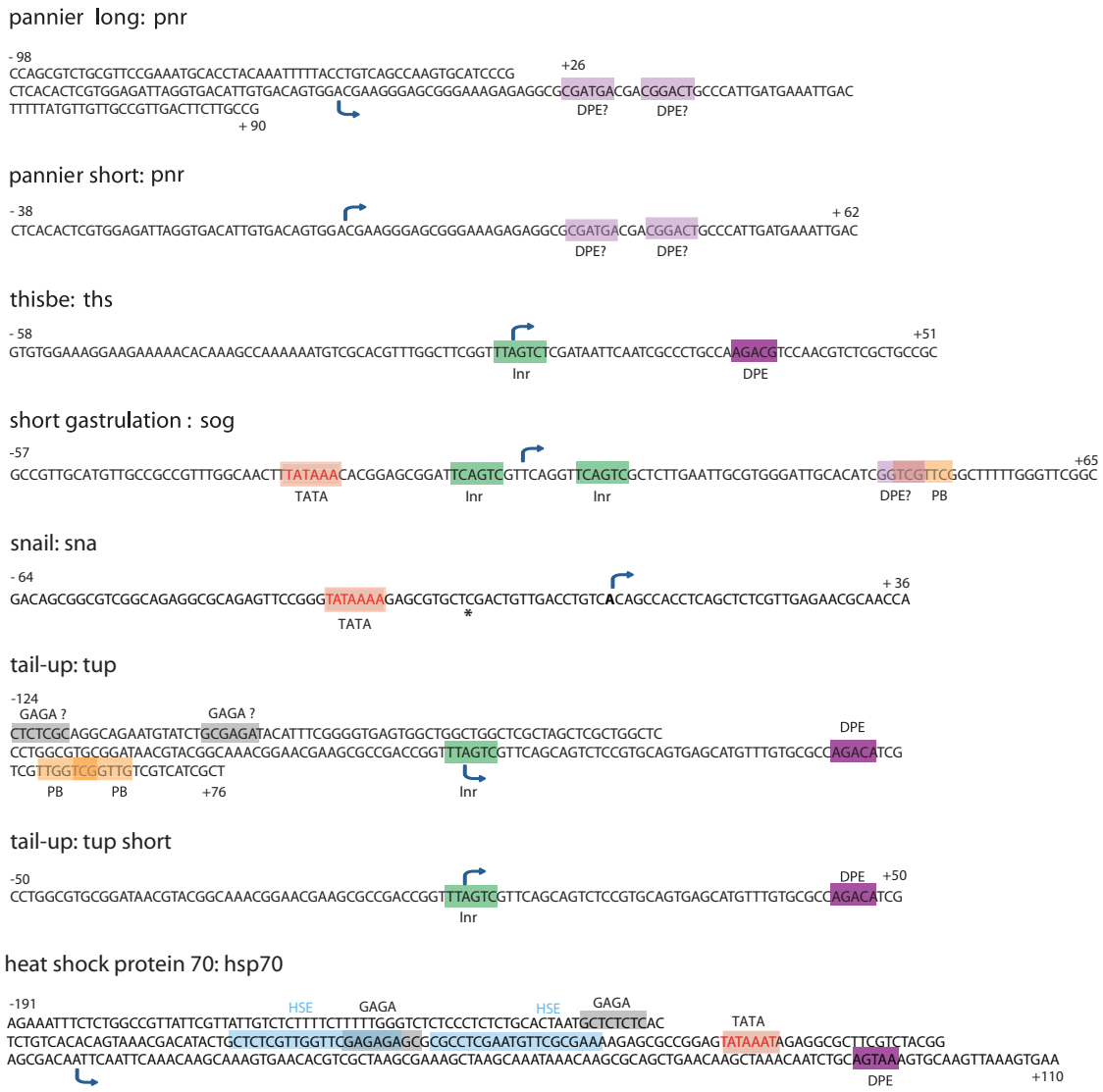

Figure S3. Minimal Promoters Examined in This Study, Related to Figures 1, 2, 3, and 4

The sequences of the promoters used in this study are provided in this Figure. Some core promoter motifs (Juven-Gershon and Kadonaga, 2010), like the INR, DPE, GAGA, TATA have been highlighted. When the sequence of the documented consensus is not perfectly respected, a ''?'' has been added. For *tup*, a larger promoter sequence has been designed to include the distal GAGA element (200bp). For consistency, two transgenic lines where created for *pnr*: one with a long *pnr* promoter sequence (188bp) and a second one with a short *pnr* promoter (100bp). The TSS is positioned at +1, according to the annotation in Flybase. In the case of *snail*, in the course of this study, we realized that the available *sna* TSS has been misannotated, and we therefore represent it with an asterisk (*). The real TSS that we determined by 5′RACE PCR, is shown as well.

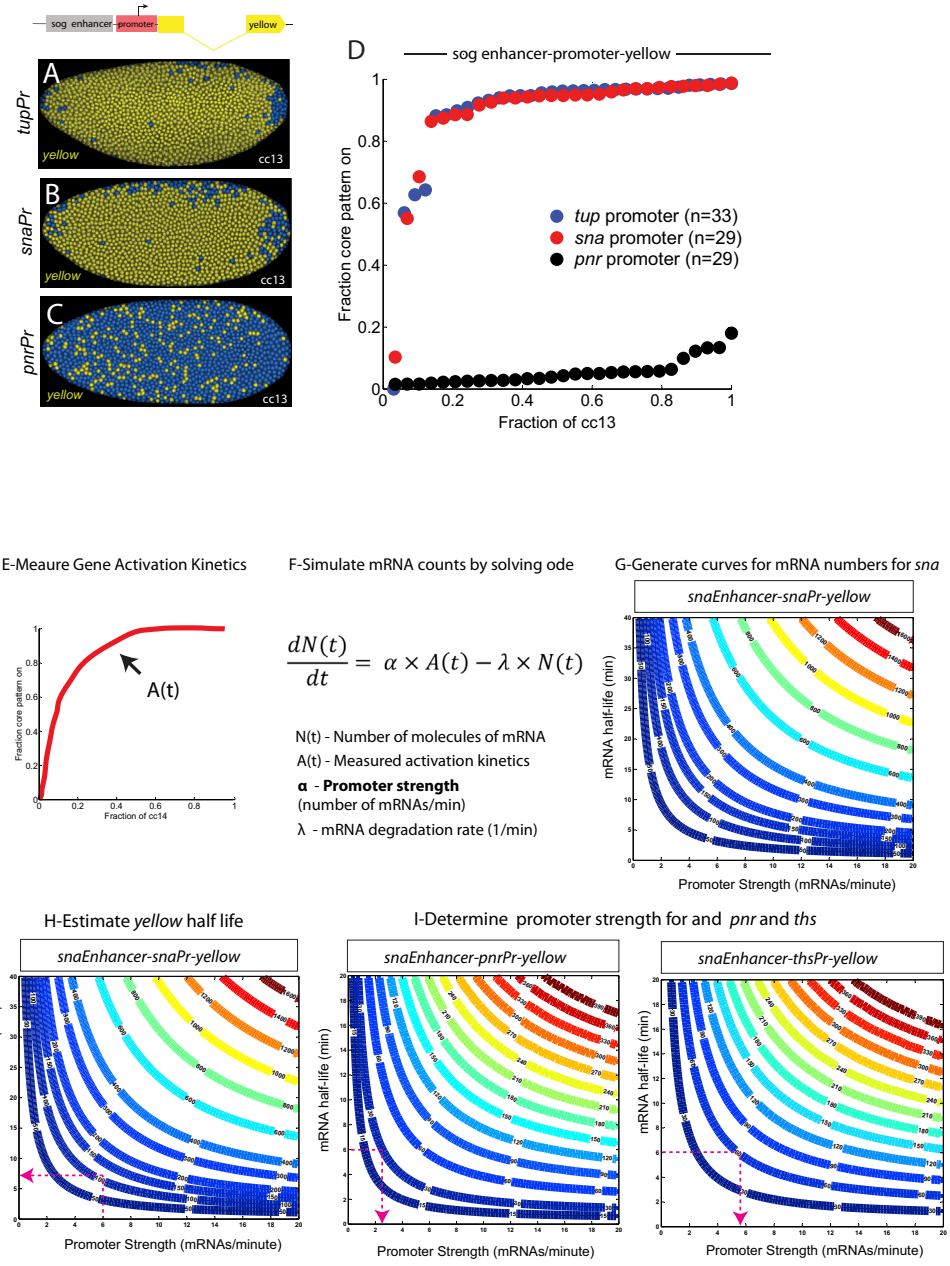

Figure S4. Temporal Coordination Profiles with the *sog* Enhancer and Measuring and Modeling mRNA Levels, Related to Figure 4

(A–C) Processed images showing ventral views of embryos after fluorescent in situ hybridization using a *yellow* intronic probe showing nascent transcripts from a *sog* enhancer-*tup* promoter (A) transgenic embryo or from a *sog* enhancer-*sna* promoter embryo (B) and a *sog* enhancer-*pnr* promoter (C) examined at cc13 (the activity of the *sog* intronic enhancer starts at the onset of cc13 and during this time period the gene is not repressed by Snail).

(D) Quantification of the dynamics of de novo transcription in these *sog* enhancer transgenic lines.

(E) Graph illustrating the activation curves measured for a given construct.

(F) Ordinary Differential Equation (ODE) used to estimate the average number of mRNA molecules per cell as a function of time.

(G) Curves for different means of mRNA counts obtained for the *snaE-snaPromoter-yellow* minigene. These curves are obtained by using (E) and (F).

(H) Knowing that the promoter strength for *snail* is about 6 mRNA/min (Boettiger and Levine, 2013) and that the mean number of *yellow* full-length mRNA at the end of cc14 is about 100 molecules per nuclei, we determine the half-life of our reporter.

(I) Knowing the number of mRNA molecules and the half-life of the *yellow* reporter, we determine the promoter strength for *pnr* and *ths*.

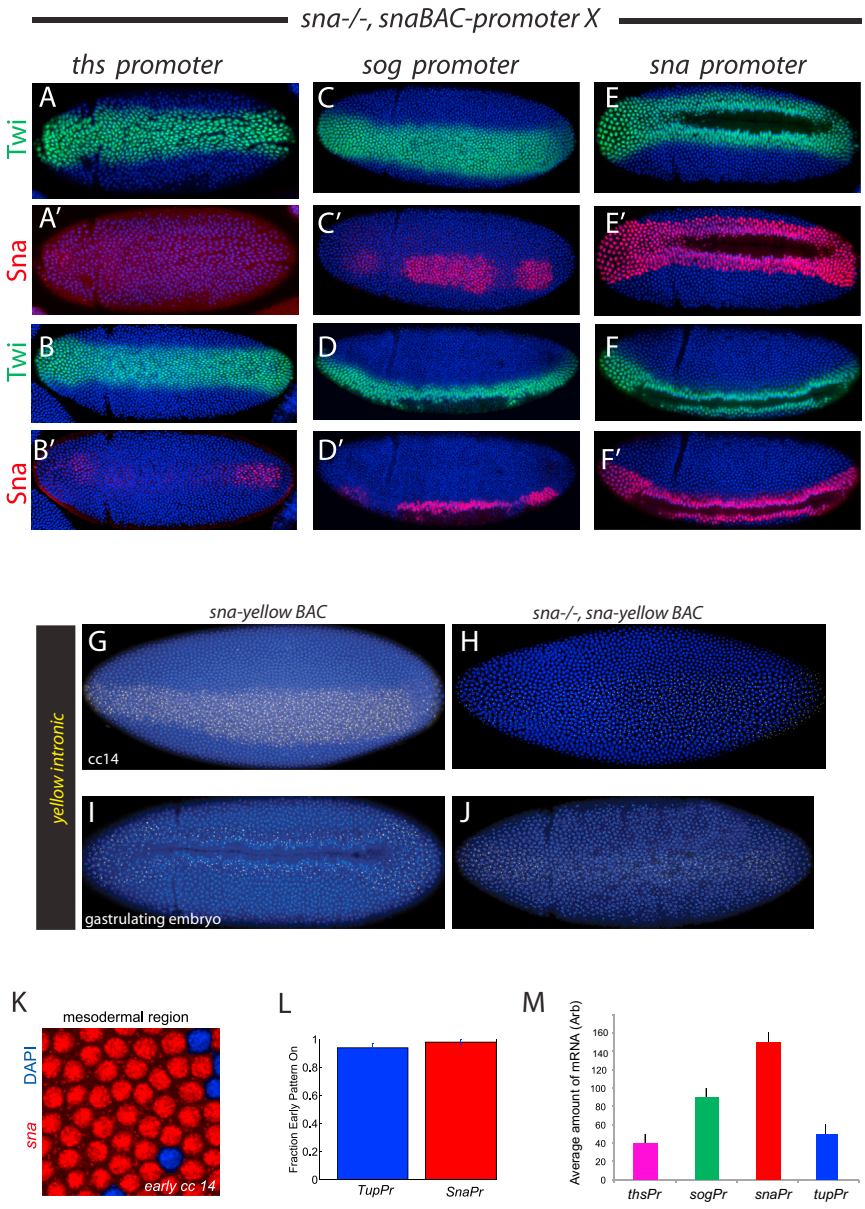

Figure S5. Stochastic Expression of *snail* Results in Gastrulation Defects; Evidence for Snail Autoregulation and Manipulation of *snail* Expression Using a Highly Paused Promoter, Related to Figures 5 and 6

(A–F) Twist (green) and Snail (red) (A′–F′) protein immunostainings for various transgenic embryos at gastrulation stage when snail expression is driven by the *ths* promoter (A and B), the moderately paused *sog* promoter (C and D) or the native *sna* promoter (E and F).

(G–J) Transgenic embryos carrying a *snail-yellow* BAC transgene, hybridized with a *yellow* intronic probe to detect nascent transcripts. (G and I) Reporter expression in control embryos at early cc14 (G) or gastrulation stage (I) when the ventral furrow is invaginating. (H and J) Reporter expression in *snail* deficient embryos (*sna*−/−). While *yellow* mRNA are normally detected early (H), reporter expression is perturbed in the absence of *snail* (J) at the time of invagination even if *snail's* major activators (Dorsal, Twist) are normally expressed.

At the onset of cc14, *snail* transcription driven by a sna-tup BAC transgene is very coordinated (K and L). Quantification of *snail* mRNA ~15 min into cc 14 reveals that the *tup* promoter produces 5 times less mRNA than the native *sna* promoter (M). Error bars represent SD.

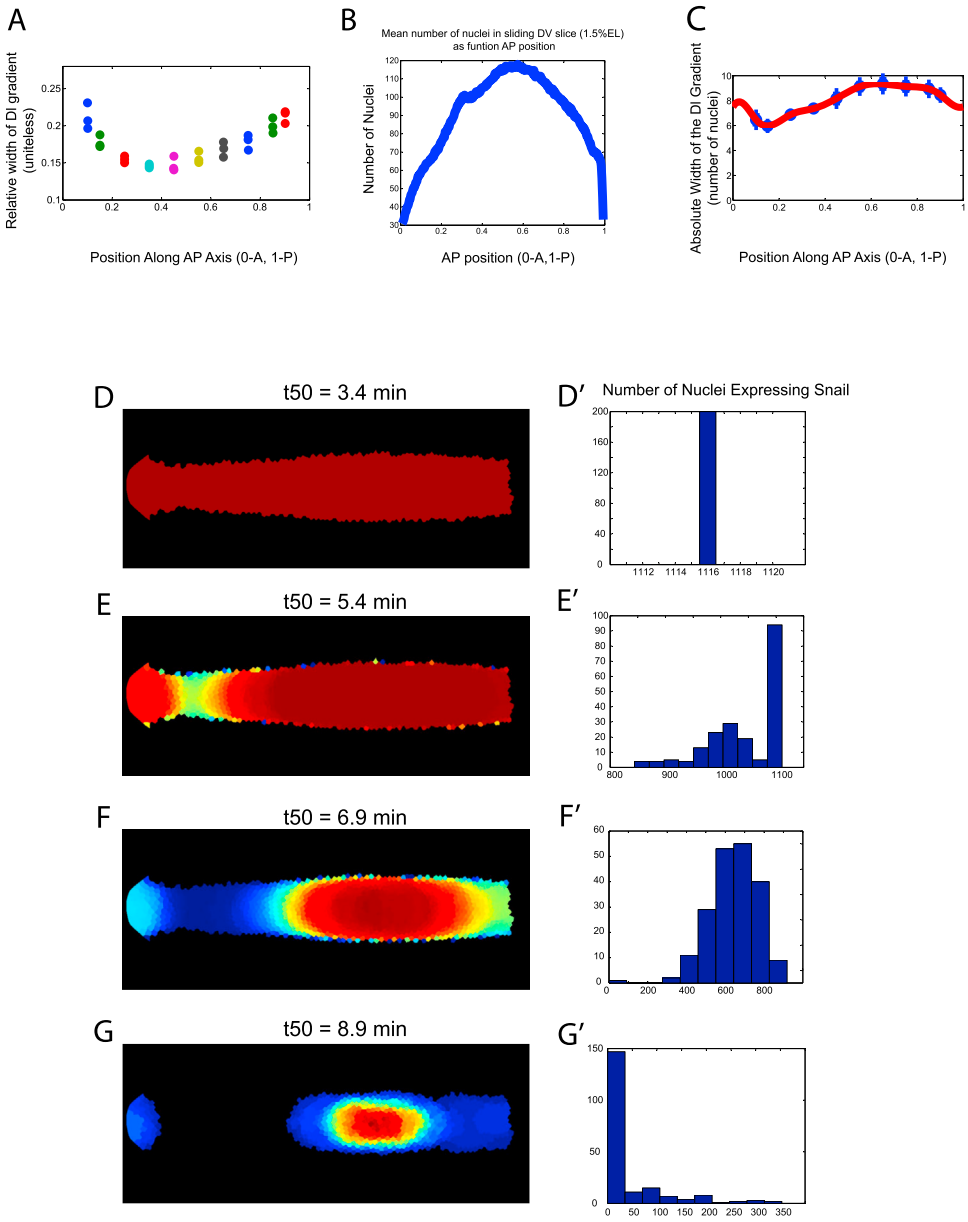

Figure S6. Spatial Profile of the Dorsal Gradient and Statistics on Model Behavior, Related to Figure 6

(A) Relative width of the Dorsal gradient as measured at different positions along the embryo (taken directly from Kanodia et al., 2011).

(B) Mean number of nuclei in a 1.5% EL slice of the embryo running from anterior to posterior for 42 embryos downloaded from the Berkeley *Drosophila* Group Database (Fowlkes et al., 2008).

(C) By combining the data shown in (A) with that in (B) one can determine the width the Dorsal gradient in terms of number of cells shown in which is used in the simulations.

For each shown t50 value, 200 independent simulations were conducted and the model behavior analyzed. The false colored embryos show how frequently a particular nucleus had snail expression at the end of the simulation (Dark red to dark blue, more frequent to less frequent). These histograms show how many embryos had a particular number of nuclei expressing Snail.

(D and D′) When t50 is only 3.4 min all the simulations converge to the same point, where both the number and spatial domain of Snail expression is the same for all runs.

(E and E′) As the t50 is increased to 5.4 min, one starts to see significant variability in the spatial profile and number of nuclei expressing Snail.

(F and F′) For a t50 value of 6.9 min, the variability is so large that some embryos show a full domain of Snail expression while others loose it completely.

(G and G′) As t50 is increased even further, the Snail pattern starts to break up significantly and often disappears entirely.

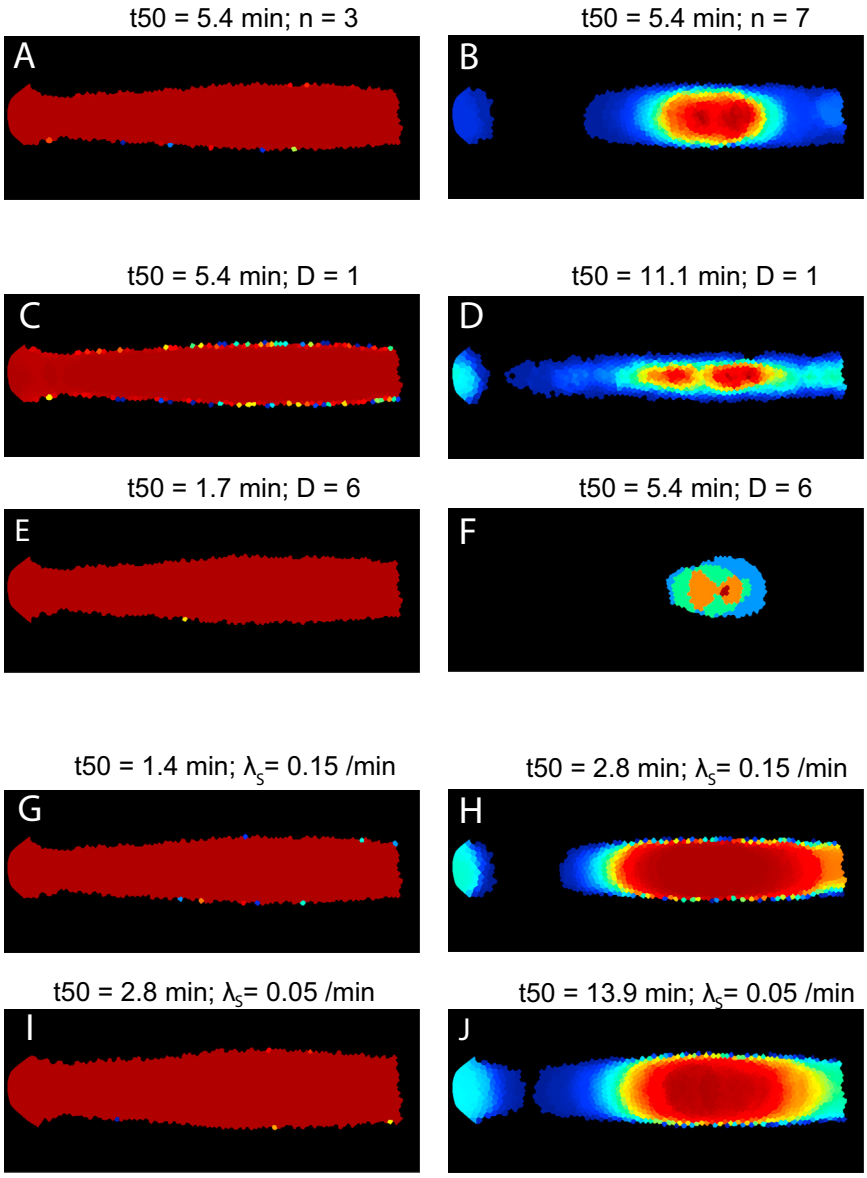

Figure S7. Model Sensitivity Analysis of Key Parameters, Related to Figure 6

As in Figure S6, 200 independent simulations were conducted and the model behavior analyzed. The false colored embryos show how frequently a particular nucleus had Snail expression at the end of the simulation (Dark red to dark blue, more frequent to less frequent). The parameter values that are not given on each panel were assigned values that were used in the default simulation as shown in Figure S6.

(A and B) Embryo histograms showing how changing the degree of cooperativity (n), affects model behavior for a given t50 value, (Figure 6E shows an equivalent simulation for n = 5).

(C and D) Embryo histograms showing how reducing the diffusion constant (D) from 3 to 1 changes model behavior, (Figure S6E shows simulations for a diffusion constant value of 3).

(E and F) Embryo histograms showing how increasing the diffusion constant from 3 to 6 affects model behavior (Figure S6E shows simulations for a diffusion constant value of 3).

(G and H) Embryo histograms showing how increasing the degradation rate of the Snail protein (λ_S) from 0.1/min to 0.15/min changes model behavior (Figure S6E shows simulations for a degradation rate of 0.1/min).

(I and J) Embryo histograms showing how decreasing the degradation rate of the Snail protein from 0.1/min to 0.05/min changes model behavior, (Figure S6E shows simulations for a degradation rate of 0.1/min).